Reprint from *Many-body Theory of Atomic Structure and Photoionization*
Edited by T. N. Chang
World Scientific, Singapore, 1993

Chapter 8

B-Spline Based Configuration-Interaction Approach for Photoionization of Two-electron and Divalent Atoms

Tu-nan Chang

Department of Physics and Astronomy
University of Southern California, LA, CA 90089-0484, U.S.A.

B-Spline-Based Configuration-Interaction Approach for Photoionization of Two-electron and Divalent Atoms

T. N. Chang

Department of Physics and Astronomy
University of Southern California
Los Angeles, CA 90089-0484, U.S.A.

1. Introduction

Recent applications of high resolution intense lasers (see, e.g., Chapter 11 of this volume) have opened up opportunities for detailed studies of multi-electron interactions involving two strongly interacting electrons outside a closed shell ^1S core of a divalent atom. Elaborate experiments in shorter wavelength regions have also been carried out with more advanced applications of the synchrotron radiation to highly correlated atomic systems (see, e.g., Chapters 10 and 12 of this volume). In addition, operating at high synchrotron radiation intensity, Domke, Remmers, and Kaindl [1] have recently observed the doubly-excited 2pnd ^1P series of He below the He^+ N=2 threshold with an improvd energy resolution of $\cong$ 4meV. Parallel to the fast growing experimental advances, significant progress have also been made in many of the existing theoretical approaches, which are capable of elucidating quantitatively the many-electron effects in photoionization. Some of the recent theoretical developments are reviewed in Chapters 1, 3, and 5-7 of this volume.

For a transition originated from a *bound* state confined in a finite volume to a continuum extending to infinity, a complete characterization of the asymptotically oscillating continuum wave functions is not necessarily required if the transition is dominated by the short-range interaction. In fact, the transition matrix can be evaluated accurately with an *effective* continuum wave function, which is a linear combination of a L^2 integrable basis confined in a finite volume and normalized with proper boundary condition consistent with its asymptotoic behavior at a large distance. Earlier attempts have been made by Heller, Reinhardt, and co-workers [2], which have led to successful applications to electron-hydron scattering and photoejection of one and two electron from H^-. Using an L^2 calculational procedure, Moccia and Spizzo [3] (see, also, Chapter 7 of this volume) have successfully represented the continuum spectrum by a set of elaborate one-electron orbitals including a modified Slater-type orbitals (STO) with an explicit $cos(kr)$ dependence. In addition, Martin and co-workers [4] have employed the usual STO basis to determine the phase shifts of the continuum wave functions with an elaborate fitting procedure. The earlier multiconfiguration Hartree-Fock (MCHF) approach for the continuum has also been extended to study the resonance structure for the photoionization of

He [5] (see, Chapter 6 of this volume). The purpose of this chapter is to review the basic theoretical features of an alternative L^2 method, i.e., a B-spline-based configuration-interaction method for *continuum spectrum* (CIC) [6], which has been applied recently with success to photoionization of a two-electron atom [7] and the single and multiphoton ionization of a divalent atom [8].

In Section 2 we present the basic procedure of the B-spline-based configuration-interaction (CI) procedure, including the use of frozen-core Hartree-Fock (FCHF) orbitals for divalent atoms. In Section 3 we extend the basic procedure outlined in Section 2 to *continuum spectrum*, including detailed discussion on calculational procedures for the scattering phase shifts, the energies and widths of the doubly excited resonant series, and the single- and multiphoton ionization cross sections. Applications to two-electron atoms and divalent atoms are presented in Section 4.

2. Basic Theoretical Procedure

Within the Breit-Pauli approximation [9], the total Hamiltonian is given by

$$H = H_{nr} + H_m \tag{1}$$

where H_m is the sum of all relativisitic contributions represented by terms given by Eqs. (3-7) in chapter 4 of this volume. The N-electron nonrelativistic Hamiltonian in atomic unit is given by

$$H_{nr}(\vec{r}_1, \vec{r}_2, \cdots) = \sum_{i=1}^{N} \left(-\frac{1}{2}\frac{d^2}{dr_i^2} - \frac{Z}{r_i} + \frac{1}{2}\frac{\vec{\ell}^{\,2}}{r_i^2} \right) + \sum_{i<j}^{N} \frac{1}{r_{ij}} \tag{2}$$

where $\vec{\ell}$ is the one-particle orbital angular momentum operator and Z is the nuclear charge. In a simple configuration-interaction (CI) calculation, the energy eigenvalue and the state wave function corresponding to an energy eigenstate of a two-electron or a divalent atom can be evaluated by diagonalizing the Hamiltonian matrix constructed from a basis set consisting of J-dependent *basis function* $\psi^{\Omega}_{n\ell n'\ell'}(\vec{r}_1, \vec{r}_2, \cdots)$. The *basis function* $\psi^{\Omega}_{n\ell n'\ell'}$ is characterized by a two-electron configuration $(n\ell, n'\ell')$ and a set of quantum numbers $\Omega \equiv (SLJM_J)$, where S is the total spin, L is the total orbital angular momentum, and J and M_J are the total angular momentum and its magnetic quantum number, respectively. The *J-dependent* basis function $\psi^{\Omega}_{n\ell n'\ell'}$ is, in turn, expressed as a sum of *J-independent* basis function $\psi^{\Lambda}_{n\ell n'\ell'}$ over all M_S and M [10], i.e.,

$$\psi^{\Omega}_{n\ell,n'\ell'} = \sum_{M_S,M} (-1)^{L-S} (2J+1)^{1/2} \begin{pmatrix} S & L & J \\ M_S & M & -M_J \end{pmatrix} \psi^{\Lambda}_{n\ell,n'\ell'}, \tag{3}$$

where $\Lambda \equiv (SLM_SM)$ represents a set of quantum numbers S, L, M_S, and M. M_S and M are the magnetic quantum numbers of S and L, respectively. Within the central field approximation, the basis function $\psi^{\Lambda}_{n\ell,n'\ell'}$ can be expressed as a sum of N-particle Slater determinant wave functions over all magnetic quantum numbers in the form of [11]

$$\psi^{\Lambda}_{n\ell,n'\ell'}(\vec{r}_1,\vec{r}_2,\cdots) = \sum_{\text{all } m's} (-1)^{\ell'-\ell}[(2S+1)(2L+1)]^{1/2} \begin{pmatrix} \ell & \ell' & L \\ m & m' & -M \end{pmatrix} \begin{pmatrix} \frac{1}{2} & \frac{1}{2} & S \\ m_s & m'_s & -M_S \end{pmatrix} \phi^{mm_sm'm'_s}_{n\ell,n'\ell'}(\vec{r}_1,\vec{r}_2,\cdots), \quad (4)$$

where the Slater-determinant wave function is constructed from the one-electron orbitals u_β, i.e.,

$$\phi^{mm_sm'm'_s}_{n\ell,n'\ell'}(\vec{r}_1,\vec{r}_2,\cdots) = (N!)^{-1/2}\, det_N \mid u_\beta(\vec{r}_\mu) \mid, \quad (5)$$

and β represents the quantum numbers n_β,ℓ_β,m_β, and m_{s_β}, which define the one-electron orbital function. More specifically, $u_{n\ell mm_s}$ is given by the product of its spatial and spin parts, i.e.,

$$u_{n\ell mm_s}(\vec{r}) = \frac{\chi_{n\ell}(r)}{r} Y_{\ell m}(\theta,\varphi)\,\sigma(m_s). \quad (6)$$

The only component in the basis functions that is not predetermined is the radial part χ of the one-particle orbital function u. As a result, this simple CI procedure is essentially non-variational and its success depends critically on the choice of χ in the construction of the Hamiltonian matrix.

2.1. *Hamiltonian Matrix and Frozen-core Hartree-Fock Approximation*

For a divalent atom of N electrons, the orbital functions for the N-2 core electrons are given by the first N-2 of the u_β's in Eq. (5) and the remaining two orbital functions represent the orbitals of the two valence electrons denoted by a two-electron configuration $(n\ell, n'\ell')$. To ensure the normalization, a factor of $1/\sqrt{2}$ should be added to Eq. (4) when $n\ell = n'\ell'$. The nonrelativistic matrix element for H_{nr} between basis functions corresponding to a pair of two-electron configurations, $(n_\mu\ell_\mu, n_\nu\ell_\nu)$ and $(n_\delta\ell_\delta, n_\gamma\ell_\gamma)$, can be expressed as the sum of three energy terms [11], i.e.,

$$< \psi^{\Lambda}_{n_\mu\ell_\mu,n_\nu\ell_\nu} \mid H_{nr} \mid \psi^{\Lambda}_{n_\delta\ell_\delta,n_\gamma\ell_\gamma} > = \sum_{i=0}^{2} E_i(n_\mu\ell_\mu\, n_\nu\ell_\nu, n_\delta\ell_\delta\, n_\gamma\ell_\gamma), \quad (7)$$

where

$$E_0(n_\mu \ell_\mu\, n_\nu \ell_\nu, n_\delta \ell_\delta\, n_\gamma \ell_\gamma) \;=$$

$$(\delta_{n_\mu n_\delta}\delta_{n_\nu n_\gamma}\delta_{\ell_\mu \ell_\delta}\delta_{\ell_\nu \ell_\gamma} + (-1)^{L+S+\ell_\delta+\ell_\gamma}\,\delta_{n_\mu n_\gamma}\delta_{n_\nu n_\delta}\delta_{\ell_\mu \ell_\gamma}\delta_{\ell_\nu \ell_\delta})\, E^{HF}_{core}\,, \quad (8)$$

$$E_1(n_\mu \ell_\mu\, n_\nu \ell_\nu, n_\delta \ell_\delta\, n_\gamma \ell_\gamma) \;=\; \delta_{\ell_\mu \ell_\delta}\delta_{\ell_\nu \ell_\gamma}\,(\delta_{n_\mu n_\delta}\, h^{HF}_{\nu\gamma} + \delta_{n_\nu n_\gamma}\, h^{HF}_{\mu\delta}) +$$

$$(-1)^{L+S+\ell_\delta+\ell_\gamma}\delta_{\ell_\mu \ell_\gamma}\delta_{\ell_\nu \ell_\delta}(\delta_{n_\mu n_\gamma}\, h^{HF}_{\nu\delta} + \delta_{n_\nu n_\delta}\, h^{HF}_{\mu\gamma})\,, \quad (9)$$

$$E_2(n_\mu \ell_\mu\, n_\nu \ell_\nu, n_\delta \ell_\delta\, n_\gamma \ell_\gamma) \;=$$

$$(-1)^{\ell_\nu-\ell_\delta}\,[\sum_k (-1)^L \begin{Bmatrix} \ell_\mu & \ell_\nu & L \\ \ell_\gamma & \ell_\delta & k \end{Bmatrix} < n_\mu \ell_\mu, n_\nu \ell_\nu \parallel V^k \parallel n_\delta \ell_\delta, n_\gamma \ell_\gamma >$$

$$+ \sum_k (-1)^S \begin{Bmatrix} \ell_\mu & \ell_\nu & L \\ \ell_\delta & \ell_\gamma & k \end{Bmatrix} < n_\mu \ell_\mu, n_\nu \ell_\nu \parallel V^k \parallel n_\gamma \ell_\gamma, n_\delta \ell_\delta >]\,, \quad (10)$$

and

$$h^{HF}_{\nu\gamma} \;=\; \int dr\, \chi_{n_\nu \ell_\nu}(r)\, h^{HF}_{\ell_\gamma}(r)\, \chi_{n_\gamma \ell_\gamma}(r)\,. \quad (11)$$

The total Hartree-Fock energy E^{HF}_{core} for the N-2 core electrons is evaluated by using the radial functions $\chi_{n_0\ell_0}$ of the occupied core orbitals, where $\chi_{n_0\ell_0}$ satisfy the eigenequation

$$h^{HF}_{\ell_0}\, \chi_{n_0\ell_0} \;=\; \epsilon_{n_0\ell_0}\, \chi_{n_0\ell_0}\,. \quad (12)$$

The one-particle Hartree-Fock Hamiltonian is given by

$$h^{HF}_\ell(r) \;=\; (-\frac{1}{2}\frac{d^2}{dr^2} - \frac{Z}{r} + \frac{1}{2}\frac{\ell(\ell+1)}{r^2}) + V^{FCHF}_\ell(r)\,, \quad (13)$$

and the frozen-core Hartree-Fock (FCHF) potential is defined explicitly by [11]

$$V^{FCHF}_\ell(r)\, f_\ell(r) \;=\; \sum_{n_0\ell_0}^{core} 2\,[\frac{2\ell_0+1}{2\ell+1}]^{1/2}\,(\ell \parallel V^0(\chi_{n_0\ell_0}, \chi_{n_0\ell_0}; r) \parallel \ell)\, f_\ell(r)$$

$$-\frac{1}{2\ell+1}\sum_{n_0\ell_0}^{core}\sum_\nu (-1)^\nu\,(\ell \parallel V^\nu(\chi_{n_0\ell_0}, f_\ell; r) \parallel \ell_0)\, \chi_{n_0\ell_0}(r), \quad (14)$$

where

$$(\ell \parallel V^{\nu}(a,b;r) \parallel \ell') \;=\; (\ell \parallel C^{[\nu]} \parallel \ell')(\ell_a \parallel C^{[\nu]} \parallel \ell_b)$$

$$\int_0^{\infty} ds\, a(s)b(s)\frac{r_<^{\nu}}{r_>^{\nu+1}}. \qquad (15)$$

The two-particle Coulomb matrix in Eq. (10) is expressed in terms of the radial integral

$$< ab \parallel V^{\nu} \parallel cd >= \int_0^{\infty} dr\, \chi_a(r)(\ell_a \parallel V^{\nu}(\chi_b, \chi_d; r) \parallel \ell_c)\, \chi_c(r)\,. \quad (16)$$

and $(\ell \parallel C^{[\nu]} \parallel \ell')$ in Eq. (15) is the reduced matrix element of the tensor operator $C^{[\nu]}$ for spherical harmonics, i.e., given explicitly by

$$(\ell \parallel C^{[\nu]} \parallel \ell') \;=\; (-1)^{\ell}[(2\ell+1)(2\ell'+1)]^{1/2} \begin{pmatrix} \ell & \nu & \ell' \\ 0 & 0 & 0 \end{pmatrix}. \qquad (17)$$

In a frozen-core Hartree-Fock (FCHF) approximation, all radial functions χ included in the Hamiltonian matrix calculation are also generated from Eq. (12), and the total Hartree-Fock core energy E_{core}^{HF} is a constant, which can be set to zero for simplicity. As a result, the nonrelativistic Hamiltonian matrix element reduces to a simple expression:

$$< \psi^{\Lambda}_{n_\mu \ell_\mu, n_\nu \ell_\nu} \mid H_{nr} \mid \psi^{\Lambda}_{n_\delta \ell_\delta, n_\gamma \ell_\gamma} >=$$

$$(\delta_{n_\mu n_\delta}\delta_{n_\nu n_\gamma}\delta_{\ell_\mu \ell_\delta}\delta_{\ell_\nu \ell_\gamma} + (-1)^{L+S+\ell_\delta+\ell_\gamma}\delta_{n_\mu n_\gamma}\delta_{n_\nu n_\delta}\delta_{\ell_\mu \ell_\gamma}\delta_{\ell_\nu \ell_\delta})(\epsilon_{n_\mu \ell_\mu} + \epsilon_{n_\nu \ell_\nu})$$

$$+ E_2(n_\mu \ell_\mu\, n_\nu \ell_\nu, n_\delta \ell_\delta\, n_\gamma \ell_\gamma)\,. \qquad (18)$$

By using the predetermined one-particle orbital functions, such as the FCHF radial functions generated by Eq. (12), the CI approach discussed above is carried out without the optimization procedure for each energy eigenstate, which is required in other more elaborate CI methods. In spite of its simplicity, a direct applications of this approach is limited by its inability to include the positive-energy orbitals in the basis functions due to the numerical difficulty in the calculation of the two-electron matrix $< ab \parallel V^{\nu} \parallel cd >$ resulting from the long-range behavior of the Coulumb interaction. In most of the earlier applications (e.g., *truncated-diagonalization method or TDM approach* [12,13]), the basis functions are limited to the products of two negative-energy (bound) one-electron orbitals (i.e., BB-type). The CI contribution from the positive-energy (continuum) orbitals, in terms of basis functions including products of bound-continuum (BC-type) and continuum-continuum (CC-type) orbitals, is often excluded due to the numerical consideration, even for highly correlated systems. This quantitative obstacle can be conveniently circumvented if one

replaces the incomplete set of *bound-only* one-electron orbital functions by a nearly *complete* set of finite L^2 basis functions, which includes both bound and continuum one-electron orbital functions confined in a finite radius R. In practice, the radius R should be larger than the estimated physical size of the energy eigenstates of our interest.

For a divalent atom, a straightforward application of the FCHF-based CI procedure will only take into account the multi-electron interactions for the two valence electrons outside a closed shell ^{1}S core. The contribution from the intrashell core excitation and the intershell core-valence interaction [14] to the energy eigenvalue is often represented by a parametrized long-range dipole core-polarization potential in the form of [14-17]

$$V_p = -\frac{\alpha}{r^4}\left[1 - e^{-(r/r_0)^6}\right] \tag{19}$$

where α is the static dipole polarizability and r_0 is a cut-off parameter for V_p as r approaches zero. For a more detailed calculation, a short-range interaction [14,16]

$$V_s = \sum_{\mu=0}^{2} a_\mu r^\mu e^{-\beta_1 r} + \sum_{\mu=0}^{2} b_\mu r^\mu e^{-\beta_2 r} \tag{20}$$

is also included to account for the additional interactions (e.g., the relativistic effects) involving the core electrons. Following a detailed calculation, Chang and Chung [14] have concluded that the combined use of V_p and V_s to represent the core-related interactions is well supported except for those dynamical properties closely associated with the small r behavior of the radial functions.

2.2. *B-Spline-Based Finite Basis Set*

The ability of the B-Spline-based finite basis set to account for the many-body interactions in atomic process was first demonstrated *explicitly* in a recent relativistic many-body perturbation application by Johnson *et al* [18]. Unlike the Slater-type orbitals, which favor the small r region, the B splines, with similar amplitude between $r = 0$ and $r = R$, tend to treat the entire physical region more uniformly. Another key advantage in the application of B splines is its independence of any *a priori* procedure in selecting the nonlinear parameters for the exponential functions. Detailed discussion of the basic properties of B splines can be found elsewhere [18-20]. The present discussion will be limited to those features related to the calculation of the one-particle radial functions χ employed in the construction of the CI basis functions.

In a bound state calculation, the set of B splines of order K and total number n is often defined with an exponentially increasing knot sequence[18,20]. The choice of such a knot sequence satisfies the need for a *densely* populated B splines near the nucleus in order to accommodate the fast raising inner s-orbitals at small r. On the other hand, a more *evenly* populated B splines at larger r is required if the oscillating behavior of the positive energy orbitals at large distance can also be

adequately represented. As a result, for transitions involving both a bound state and a continuum, we have chosen a sine-like knot sequence d_ν defined by [6]

$$d_\nu = R\ sin[\frac{\pi}{2}(\frac{(\nu-1)\Delta h}{R})^y]; \quad \nu = 1, 2, \cdots, n-K+2, \tag{21}$$

where $\Delta h = R/(n-K+1)$. The distribution of knot points can be adjusted by changing the position of the first non-zero knot d_2, which in turn determines the value of y according to Eq. (21). By employing such a knot sequence, we are able to limit the size of B-spline set to a modest n in our calculation. At the same time, we are able to take into account both the small- and large-r behavior of the orbital functions.

The nonrelativistic radial functions χ usually satisfy an eigenequation, e.g., Eq. (12), in the form of

$$-\frac{1}{2}\frac{d^2\chi}{dr^2} + V(r)\,\chi = \epsilon\,\chi \tag{22}$$

where the potential $V(r)$ is non-local in general. The solution χ is expanded in terms of a set of B splines defined between $r = 0$ and $r = R$, i.e.,

$$\chi(r) = \sum_{i=1}^{n} c_i\, B_i(r)\,. \tag{23}$$

The index K is omitted from the functions B_i for simplicity. At the endpoints $r = 0$ and $r = R$, all B splines equal zero except for B_1 and B_n, i.e.,

$$B_1(r=0) = 1 \quad \text{and} \quad B_n(r=R) = 1\,. \tag{24}$$

In our calculation, the radial functions χ are subject to the nonrelativistic boundary conditions, $\chi(0) = \chi(R) = 0$, which can be satisfied if we set

$$c_1 = c_n = 0\,. \tag{25}$$

Substitution of Eqs. (23) and (25) into Eq. (22) leads to a $(n-2)\times(n-2)$ generalized eigenvalue equation:

$$H\,C = \epsilon\,A\,C\,, \tag{26}$$

where H and A are $(n-2)\times(n-2)$ matrices given by

$$H_{ij} = -\frac{1}{2} < B_i \mid \frac{d^2}{dr^2} \mid B_j > + < B_i \mid V \mid B_j >;$$

$$i \text{ and } j = 2, \ldots, (n-1)\,, \tag{27}$$

$$A_{ij} = < B_i \mid B_j >; \qquad i \text{ and } j = 2, \ldots, (n-1)\,. \tag{28}$$

The radial eigenfunction χ_ν of Eq. (22) corresponding to an energy eigenvalue ϵ_ν is given by

$$\chi_\nu(r) = \sum_{i=2}^{n-1} c_i B_i(r), \tag{29}$$

where the set of n-2 coefficients c_i forms the eigenvector,

$$C_\nu = (c_2, c_3, \ldots, c_{n-1}), \tag{30}$$

of Eq. (26).

The calculated $\epsilon_{\nu\ell}$ of the first few lowest negative-energy solutions corresponding to a specific orbital angular momentum ℓ with their eigenfunctions completely confined in a radius R should agree with the numerical results of Eq. (22) from direct integration. The positive-energy orbitals, with energy $\epsilon_{\nu\ell}$ up to few Ry, should exhibit an oscillating behavior at large r. In practice, only those positive-energy orbitals with momentum $k_{\nu\ell} = (2\epsilon_{\nu\ell})^{\frac{1}{2}}$ that satisfy the boundary conditions, $\chi_{\nu\ell}(r=0) = \chi_{\nu\ell}(r=R) = 0$, or,

$$k_{\nu\ell}R + \frac{Z}{k_{\nu\ell}} ln(2k_{\nu\ell}R) - \frac{\ell\pi}{2} + \delta_C + \delta_\ell = m\pi, \tag{31}$$

should appear in the nearly complete set of discretized radial functions $\chi_{\nu\ell}$. For a pure hydrogenic potential, i.e., if

$$V(x) = -\frac{Z}{r} + \frac{1}{2}\frac{\ell(\ell+1)}{r^2}, \tag{32}$$

the short-range phase shift δ_ℓ vanishes and δ_C equals the analytical Coulomb phase shift. Following the numerical procedure described above, the n-2 radial eigenfunctions χ_ν of Eq. (22) form the one-particle finite basis set in the CI basis functions.

In calculating the Hamiltonian matrix, the CI basis set consists of a number of two-electron *configuration series* $n\ell\ell'$. Each $n\ell\ell'$ series includes a set of basis functions $\psi^{\Lambda}_{n\ell,n'\ell'}$ corresponding to one of the valence electrons in a fixed orbital $n\ell$ and the other one with orbital angular momentum ℓ' but variable energy, both negative and positive, over an entire set of eigenfunctions χ of Eq. (22). A configuration series is in theory equivalent to an open channel in close-coupling calculation when the $n\ell$ orbital is bound. Such a series includes only the BB- and BC-type of configurations. The CC-type of configurations are included in the basis set when $n\ell$ represents a positive-energy orbital.

2.3. *State Wave Function and Energy Level*

Within the nonrelativistic FCHF approximation, the energy eigenvalue E^{Λ}_{μ} of a state $|\ \mu >$ is calculated by diagonalizing the Hamiltonian matrix given by Eq. (18). The corresponding state wave function is given by

$$\Phi^{\Lambda}_{\mu} = \sum_{\nu\ell\ell'} \Xi^{\Lambda}_{\mu,\nu\ell\ell'}, \tag{33}$$

where the *configuration series function*

$$\Xi^{\Lambda}_{\mu,\nu\ell\ell'} = \sum_{\nu'} C^{\Lambda}_{\mu}(\nu\ell, \nu'\ell')\ \psi^{\Lambda}_{\nu\ell\ \nu'\ell'} \tag{34}$$

represents the contribution to the state wave function from the $\nu\ell\ell'$ configuration series. A complete set of coefficients $C^{\Lambda}_{\mu}(\nu\ell, \nu'\ell')$ forms the eigenvector of the state $\mid \mu >$.

For a divalent atom, the calculated energy eigenvalue is denoted as $E^{\Lambda}_{n_i\ell_i\, n_o\ell_o}$ if the eigenstate $\mid \mu >$ is dominated by a two-electron configuration $(n_i\ell_i\, n_o\ell_o)$ with the inner valence electron in an $n_i\ell_i$ orbital and the outer valence electron in an $n_o\ell_o$ orbital. For simplicity, the ionization threshold with both valence electrons removed is set to have a zero energy. The calculated energy eigenvalue $E^{\Lambda}_{n_i\ell_i\, n_o\ell_o}$ corresponding to an energy eigenstate $(n_i\ell_i\, n_o\ell_o)^{\,2S+1}L$ can therefore be expressed in Ry unit in terms of the effective quantum number $\nu_{n_i\ell_i}$ leading to the $n_i\ell_i$ ionization threshold of the atomic ion, i.e.,

$$E^{\Lambda}_{n_i\ell_i\, n_o\ell_o}(N, Z) = -E^{I}_{n_i\ell_i}(N-1, Z) - \frac{Z_e^2}{\nu^2_{n_i\ell_i}}, \tag{35}$$

where $Z_e = Z - N + 1$ is the effective nuclear charge and $E^{I}_{n_i\ell_i}(N-1, Z)$ is the ionization energy required to remove the $n_i\ell_i$ electron from the corresponding atomic ion of N-1 electrons. The quantum defect is given by $\mu_{\ell_o} = n_o - \nu_{n_i\ell_i}$.

2.4. *Oscillator Strength*

For an atomic transition from an initial state $\mid a >$ to a final state $\mid b >$, the theoretical oscillator strengths in the dipole-length and dipole-velocity approximation are given by [21]

$$f^{\ell}_{ba} = \frac{1}{3g_a}\Delta E_{ba} \sum_{\text{all M's}} |< \Phi^{\Lambda_a}_a \mid \sum_{\alpha} \vec{r}_{\alpha} \mid \Phi^{\Lambda_b}_b >|^2, \tag{36}$$

and

$$f^{v}_{ba} = \frac{4}{3g_a}\Delta E^{-1}_{ba} \sum_{\text{all M's}} |< \Phi^{\Lambda_a}_a \mid \sum_{\alpha} \vec{\nabla}_{\alpha} \mid \Phi^{\Lambda_b}_b >|^2, \tag{37}$$

respectively. The transition energy

$$\Delta E_{ba} = E^{\Lambda_b}_b - E^{\Lambda_a}_a \tag{38}$$

is given in Ry unit and

$$g_a = (2S_a + 1)(2L_a + 1) \tag{39}$$

is the degree of degeneracy of the initial state. The oscillator strength f_{ba} is positive for an *absorption* when ΔE_{ba} is positive and it is negative for an *emmision* when ΔE_{ba} is negative.

For transitions involving the two outershell electrons, the sum over the square of the dipole matrix in Eqs. (36-37) can be evaluated with a straightforward application of the angular momentum algebra and the oscillator strengths in the dipole-length and dipole-velocity approximation are given by

$$f_{ba}^{\ell} = \delta_{S_b S_a} \frac{2L_b+1}{3} \Delta E_{ba} \mid F_{ba}^{\ell} \mid^2 \tag{40}$$

and

$$f_{ba}^{v} = \delta_{S_b S_a} \frac{4(2L_b+1)}{3} \Delta E_{ba}^{-1} \mid F_{ba}^{v} \mid^2 , \tag{41}$$

respectively. The oscillator strength f_{ab}^{e} for an *emission* from an upper state $\mid b >$ to a lower state $\mid a >$ is related to the oscillator strength f_{ba}^{abs} for an *absorption* from a lower state $\mid a >$ to an upper state $\mid b >$ by

$$f_{ab}^{e} = -(\frac{2L_a+1}{2L_b+1}) f_{ba}^{abs} . \tag{42}$$

The transition amplitude F_{ba} is given by

$$F_{ba} = \sum_{j,i} C_b^{\Lambda_b}(n_j' \ell_j', n_j \ell_j) \, C_a^{\Lambda_a}(n_i' \ell_i', n_i \ell_i) \, D_{ba}^{ji} , \tag{43}$$

where

$$\begin{aligned} D_{ba}^{ji} &= d_{ba}(j'j, i'i) + d_{ba}(jj', ii') + (-1)^{S_a} d_{ba}(j'j, ii') \\ &\quad + (-1)^{S_b} d_{ba}(jj', i'i) \end{aligned} \tag{44}$$

is the dipole transition matrix between configurations $(n_j' \ell_j', n_j \ell_j)$ and $(n_i' \ell_i', n_i \ell_i)$. For a configuration corresponding to two equivalent electrons, a factor of $1/sqrt2$ should be added. The matrix element d_{ba} is the product of the angular coefficient ρ and the one-particle radial integrals, i.e.,

$$\begin{aligned} d_{ba}(j'j, i'i) &= \rho(\ell_j' \ell_j \ell_i' \ell_i; \Lambda_b \Lambda_a) \\ &\quad < \chi_{n_j \ell_j} \mid \chi_{n_i \ell_i} >< \chi_{n_j' \ell_j'} \mid t \mid \chi_{n_i' \ell_i'} > , \end{aligned} \tag{45}$$

where $< \chi_{n_j' \ell_j'} \mid t \mid \chi_{n_i' \ell_i'} >$ is the one-particle radial dipole matrix and t is the radial part of the position and gradient operators in the length and velocity approximation, respectively. The overlapping integral $< \chi_{n_j \ell_j} \mid \chi_{n_i \ell_i} >= \delta_{n_j n_i} \delta_{\ell_j \ell_i}$ in the FCHF approximation. The angular factor ρ is given by

$$\begin{aligned} \rho(\ell_1 \ell_2 \ell_3 \ell_4; \Lambda_b \Lambda_a) &= (-1)^{\ell_1} \delta_{\ell_2 \ell_4} [(2\ell_1+1)(2\ell_3+1)]^{1/2} \\ &\quad \begin{pmatrix} \ell_1 & 1 & \ell_3 \\ 0 & 0 & 0 \end{pmatrix} \begin{Bmatrix} L_a & 1 & L_b \\ \ell_1 & \ell_4 & \ell_3 \end{Bmatrix} , \end{aligned} \tag{46}$$

where Λ_α represents the quantum numbers S, L, M_S, and M associated with the state $\mid \alpha >$.

3. Configuration-Interaction Method for Continuum Spectrum

In this section we present the extension of the B-spline-based configuration-interaction procedure outlined in previous section to continuum spectrum for a two-electron or a divalent atom with a $ns^2\ ^1S$ ground state. At energy above the first ionization threshold, the spectrum is often dominated by a series of doubly excited autoionization resonances embedded in a single continuum open-channel $ns\ell$. Following the notation employed in Eqs. (33-34), the state wave function Φ^{Λ}_{E} can be separated into two parts, i.e.,

$$\Phi^{\Lambda}_{E} = \Xi^{\Lambda}_{E,ns\ell} + \sum_{\mu_0\ell_0\ell'} \Xi^{\Lambda}_{E,\mu_0\ell_0\ell'}, \tag{47}$$

where the first term represents the $ns\ell$ ionization channel and the second term denotes the combined contribution from doubly excited configurations from all closed channels. The kinetic energy ϵ and the momentum k of the ionized electron are given by

$$\epsilon = \frac{1}{2}k^2 = E + E_I, \tag{48}$$

where E_I is the ionization energy of the remaining ns electron after the removal of the first ns electron.

3.1. *Continuum Function at Large r*

Asymptotically, in a direct scattering calculation, the correct wave function of an outgoing ℓ electron with momentum k is given by

$$(\frac{2}{\pi k})^{\frac{1}{2}}\ sin\ [kr + \frac{q}{k}ln(2kr) - \frac{\ell\pi}{2} + \delta_C + \delta_\ell] \tag{49}$$

as $r \rightarrow \infty$, where q is the effective nuclear charge experienced by the outgoing electron and δ_ℓ is the scattering phase shift due to the short range interaction. The scattering phase shift can be extracted from the present calculation by comparing the oscillating part of the configuration series function $\Xi^{\Lambda}_{E,ns\ell}$ for the $ns\ell$ open-channel with the asymptotic expression given by Eq. (49). We first express the configuration series function $\Xi^{\Lambda}_{E,ns\ell}$ in a form identical to the Slater determinant function $\psi^{\Lambda}_{ns\xi_{\epsilon\ell}}$, where one of the radial functions is replaced by a one-particle radial function

$$\xi_{\epsilon\ell}(r) = \sum_{\nu} C^{\Lambda}_{E}(ns, \nu\ell)\chi_{\nu\ell}(r). \tag{50}$$

The numerical function $\xi_{\epsilon\ell}(r)$ is then matched at a finite r against an asymptotic expression employed by Burgess, i.e., [22]

$$\xi_{\epsilon\ell}(r) \longrightarrow A\ [\frac{k}{\zeta(r)}]^{\frac{1}{2}}\ sin[\phi(r) + \delta_\ell] \tag{51}$$

as $r \rightarrow R$, where ς and ϕ are functions of r. As $r \rightarrow \infty$, $\varsigma \rightarrow k$ and

$$\phi \longrightarrow (kr + \frac{q}{k} ln(2kr) - \frac{\ell\pi}{2} + \delta_C). \tag{52}$$

An accurate representation of the continuum by discretized finite basis set depends critically on the matching between the calculated raidal function and the correct asymptotic expression over a large portion of r with a constant amplitude A. The application of the present procedure to the electron-hydrogen scattering below the $n = 2$ threshold has led to a nearly perfect matching between our calculated $\xi_{\epsilon\ell}(r)$ and Eq. (51) (see, e.g., Fig. (1) of Ref. [6]). As a result, the scattering phase shift δ_ℓ can be determined easily without the help from any elaborate fitting procedure such as the one proposed by Martin and Salin [3].

For a two-electron or a divalent atom, the effective nuclear charge q in Eq. (52) equals $Z - 1$, even when $\xi_{\epsilon\ell}(r)$ is actually a sum of one-particle radial functions which are subject to a nuclear charge of Z asymptotically. At energy near a doubly excited resonance, the phase shift $\delta_\ell(E)$ is given by

$$\delta_\ell(E) = \delta_\ell^b(i_{max}; E) + \delta_\ell^r(E_r, \Gamma; E), \tag{53}$$

where the smooth varying $\delta_\ell^b(i_{max}; E)$ can be expressed in terms of a simple polynomial expansion

$$\delta_\ell^b(i_{max}; E) = \sum_{i=0}^{i_{max}} a_i E^i, \tag{54}$$

and $\delta_\ell^r(E_r, \Gamma; E)$, which is given in the usual form

$$\delta_\ell^r(E_r, \Gamma; E) = tan^{-1} \frac{\Gamma/2}{E_r - E}, \tag{55}$$

represents a fast changing resonant part $\delta_\ell^r(E_r, \Gamma; E)$ which increases rapidly by a total of π [23,24]. As a result, a set of closely populated energy eigenvalues is required to describe the detail energy variation of the scattering phase shift across the resonance. This is carried out by repeating our calculations at slightly varied values of R. The energy E_r and the width Γ of the resonance are determined numerically by a least square fit procedure detailed in Section 3.3.

3.2. *Single- and Multiphoton Ionization*

Theoretically, when the orbital function of the outgoing electron is normalized asymptotically by Eq. (49), the cross sections (in unit of a_0^2) for the photoionization from an initial state $\mid I >$, with a photon energy E_γ given in atomic unit, are given by

$$\sigma = \frac{8}{3}\pi^2 \alpha \; g(E_\gamma) \;\; \mid D_{EI} \mid^2, \tag{56}$$

where α is the fine structure constant and $g(E) = E$ and E^{-1} for the dipole length and velocity approximations, respectively. The dipole matrix between the initial state $\mid I >$ and the final state $\mid E >$ is given by

$$D_{EI} =< \Phi_E^{\Lambda} \mid \hat{D}(1,2) \mid \Phi_I^{\Lambda} >, \tag{57}$$

where

$$\hat{D}(1,2) = D(\vec{r}_1) + D(\vec{r}_2), \tag{58}$$

and D represent the position and gradient operators for the length and velocity approximations, respectively.

When the final state wave function Φ_E^{Λ} is calculated by using the discretized finite basis set, the normalization constant $(2/\pi k)^{\frac{1}{2}}$ in Eq. (49) should be replaced by the amplitude A given in Eq. (51). As a result, Eq. (56) should be multiplied by a constant

$$N_k = \frac{2/(\pi k)}{A^2} \tag{59}$$

when we replace the dipole matrix D_{EI} by D_{EI}^d, i.e.,

$$\sigma = \frac{8}{3}\pi^2 \alpha \; g(E_\gamma) \; N_k \; \mid D_{EI}^d \mid^2 . \tag{60}$$

The new dipole matrix D_{EI}^d, also defined by Eq. (57), is evaluated using the state wave functions Φ_E^{Λ} and Φ_I^{Λ} calculated with the discretized finite basis set. Alternatively, the photoionization cross section can be expressed in terms of the oscillator strength f_{EI} for absorption by the simple relation

$$\sigma = \frac{4\pi\alpha}{kA^2} \; f_{EI}, \tag{61}$$

where f_{EI} can be calculated numerically following the same procedure for the bound-bound transitions given in Section 2.

Within the low field limit, the N-photon generalized ionization cross section σ_N in cm^{2N} sec^{N-1}, with photon energy $\hbar\omega$ and outgoing electron momentum k, is given in the lowest-order perturbation theory by [8,25]

$$\sigma_N = \frac{4}{kA^2} \frac{\alpha c}{a_o} [\frac{\omega}{F_o}]^N \sum_{J_f} \mid D^{(N)} \mid^2, \tag{62}$$

where A is the amplitude given by Eq. (51) in the CIC procedure. The summation in Eq. (62) includes contribution from all final states with allowed total angular momentum J_f. The N-photon transition amplitude $D^{(N)}$ from an initial state g to a final state f is given by [26]

$$D^{(N)} = \sum_{\nu,\mu,\cdots,\lambda} \frac{F_{f\nu} \, F_{\nu\mu} \cdots F_{\lambda g}}{[E_\nu - E_g - (N-1)\omega] \cdots [E_\lambda - E_g - \omega]} . \tag{63}$$

Except for the angular factor ρ, the transition amplitude F_{ba} is similar to the one given by Eq. (43), i.e.,

$$F_{ba} = \sum_{j,i} C_b^{\Omega_b}(n'_j\ell'_j, n_j\ell_j)\, C_a^{\Omega_a}(n'_i\ell'_i, n_i\ell_i)\, D_{ba}^{ji}\,, \tag{64}$$

where the dipole transition matrix D_{ba}^{ji} is given by Eq. (44) with its corresponding angular factor $\rho(\ell_1\ell_2\ell_3\ell_4; \Lambda_b\Lambda_a)$ in Eq. (45) replaced by $\rho(\ell_1\ell_2\ell_3\ell_4; \Omega_b\Omega_a)$, which is related to $\rho(\ell_1\ell_2\ell_3\ell_4; \Lambda_b\Lambda_a)$ by

$$\begin{aligned}\rho(\ell_1\ell_2\ell_3\ell_4; \Omega_b\Omega_a) \;=\; & (-1)^{J_b+J_a+L_b+L_a+S_a+\ell_1+\ell_2-M_{J_b}}\,\delta_{S_bS_a} \\ & [(2J'+1)(2J+1)(2L'+1)(2L+1)]^{\frac{1}{2}} \begin{pmatrix} J_b & 1 & J_a \\ -M_{J_b} & q & M_{J_a} \end{pmatrix} \\ & \begin{Bmatrix} L_b & J_b & S_a \\ J_a & L_a & 1 \end{Bmatrix} \rho(\ell_1\ell_2\ell_3\ell_4; \Lambda_b\Lambda_a),\end{aligned} \tag{65}$$

where q=0 for linearly polarized light and q=$\pm$1 for circularly polarized light.

3.3. *Computational Procedure*

The computational procedure employed in the CIC method is summarized in the flow chart shown in Figure 1. In our numerical calculations, which usually involve a few excited states in each of the doubly exicted resonant series, a radius

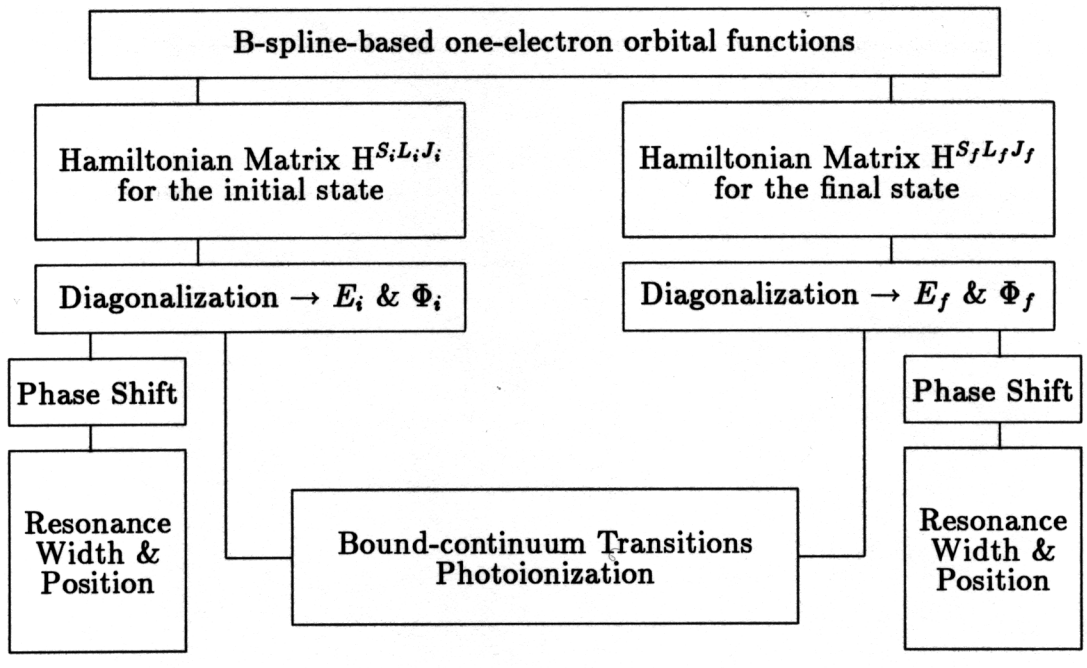

Figure 1. Computational procedure for the CIC calculation.

of $R = 120 - 140a_0$ is used. The B-spline set is generally limited to a modest size of $n = 80 - 100$ with $k = 9 - 11$. Approximately fifteen to twenty-five R values are included in a typical calculation for a complete description of a series of doubly excited resonant states.

3.3.1. *Diagonalization procedure*

Although it is necessary in general to include a larger number of configuration series for a highly accurate quantitative calculation, the state wave function Φ_E^A is usually dominated by a limited number of configuration series. A full diagonalization of a hamiltonian matrix with over a few thousands configurations is not only time consuming but also often unnecessary, since in practice, only a small number of energy eigenstates are of interest in our calculation. To minimize the computational effort and the hardware requirement, we have developed a diagonalization procedure similar to the standard Davidson procedure [27].

For a $N \times N$ real symmetric hamiltonian matrix constructed from a basis set $\{\psi_i;\ \mathrm{i} = 1,\ 2,\ \cdots,\ \mathrm{N}\}$, i.e., $H_{ij} =< \psi_i \mid H \mid \psi_j >$, the state wave function Φ_μ corresponding to an energy eigenvalue ϵ_μ is represented by a set of coefficients $\{c_i^\mu;\ \mathrm{i} = 1,\ 2,\ \cdots,\ \mathrm{N}\}$, i.e.,

$$\Phi_\mu = \sum_{i=1}^{N} c_i^\mu \, \psi_i. \tag{66}$$

In practice, over 99% of the probability density $\sum_i \mid c_i^\mu \mid^2$ in Φ_μ can be attributed to a *subset* of coefficients, i.e., $\{c_i^\mu,\ \mathrm{i} = 1,\ 2,\ \cdots,\ \mathrm{n}\}$, where n is much smaller than N. In the first step of our diagonalization procedure, a smaller $n \times n$ hamiltonian submatrix H^n is diagonalized fully using any standarized code, which leads to an approximate state wave function

$$\Phi_\mu^{(0)} = \sum_{i=1}^{n} a_i^\mu \, \psi_i \tag{67}$$

corresponding to an approximate energy eigenvalue $\epsilon_\mu^{(0)}$. Second, we replace the basis set $\{\psi_i\}$ by a new basis set $\{\omega_i\}$

$$\omega_i = \begin{cases} \Phi_i^{(0)} & ;i = 1, 2, \cdots, n \\ \psi_i & ;i = n+1, n+2, \cdots, N. \end{cases} \tag{68}$$

The new $N \times N$ real symmetric hamiltonian matrix, i.e., $H_{ij}^t =< \omega_i \mid H \mid \omega_j >$, is given explicitly by

$$H_{ij}^t = \begin{cases} \delta_{ij}\epsilon_j^{(0)} & ;i \ \& \ j = 1, 2, \cdots, n \\ \sum_{k=1}^{n} a_k^i \, H_{kj} & ;i = 1, 2, \cdots, n \ \& \ j = n+1, n+2, \cdots, N \\ H_{ij} & ;i \ \& \ j = n+1, n+2, \cdots, N. \end{cases} \tag{69}$$

Third, we express the state wave function corresponding to an energy eigenvalue ϵ_μ in terms of the new basis set $\{\omega_i\}$, or

$$\Phi_\mu = \sum_{i=1}^{N} b_i^\mu \, \omega_i, \tag{70}$$

where the coefficients b_i^μ satisfy the algebraic equation

$$\sum_{i}^{N} H_{ki}^t \, b_i^\mu = \epsilon_\mu \, b_k^\mu ; \quad k = 1, 2, \cdots, N \ \& \ \mu = 1, 2, \cdots, n. \tag{71}$$

The coefficient b_i^μ and the energy eigenvalue ϵ_μ can also be expressed explicitly by the equations

$$b_i^\mu = \frac{\sum_{j(\neq i)}^{N} H_{ij}^t \, b_j^\mu}{\epsilon_\mu - H_{ii}^t}; \quad i = 1, 2, \cdots, N, \tag{72}$$

and

$$\epsilon_\mu = \sum_{i,j}^{N} b_i^\mu \, H_{ij}^t \, b_j^\mu, \tag{73}$$

respectively.

Our next step is to evaluate the coefficients b_i^μ and the energy eigenvalue ϵ_μ using Eqs. (72-73) iteratively. We start by setting $\epsilon_\mu = \epsilon_\mu^{(0)}$, and

$$b_k^\mu = \begin{cases} \delta_{k\mu} & ; k = 1, 2, \cdots, n \\ \\ \frac{H_{k\mu}^t}{\epsilon_\mu - H_{kk}^t} & ; k = n+1, n+2, \cdots, N. \end{cases} \tag{74}$$

After this set of coefficients $\{b_k^\mu ; k = 1, 2, \cdots, N\}$ is normalized to unity, a new energy eigenvalue ϵ_μ is estimated using Eq. (73). We then proceed to calculate a complete set of new coefficients $\{b_k^\mu ; k = 1, 2, \cdots, N\}$ using Eq. (72). This set of coefficients is normalized to unity again before the iterative procedure is repeated until the energy eigenvalue ϵ_μ and its corresponding eigenvector $\{b_k^\mu ; k = 1, 2, \cdots, N\}$ are converged. Finally, for each ϵ_μ, a simple transformation

$$c_i^\mu = \begin{cases} \sum_{k=1}^{n} a_i^k \, b_k^\mu & ; i = 1, 2, \cdots, n \\ \\ b_i^\mu & ; i = n+1, n+2, \cdots, N \end{cases} \tag{75}$$

leads to a set of coefficients $\{c_i^\mu ;$ i = 1, 2, $\cdots$, N$\}$, which forms the state wave function Φ_μ given by Eq. (66).

3.3.2. *Resonant energy and width*

The resonant energy E_r and width Γ are determined from the energy variation of the calculated scattering phase shifts $\delta_\ell(E_k)$ using the procedure outlined in Section 3.1. Numerically, we first calculate a set of estimated $\delta_\ell^b(E_k)$ by taking the *difference* between the calculated $\delta_\ell(E_k)$ and a set of $\delta_\ell^r(E_r, \Gamma; E_k)$ calculated from Eq. (55) with a pair of estimated E_r and Γ. This set of $\delta_\ell^b(E_k)$ is, in turn, used to determine the coefficients $\{a_i\}$ in Eq. (54) by using a least square fit procedure. Second, with the fitted expansion coefficients $\{a_i\}$, we proceed to calculate a set of new $\delta_\ell^b(E_k)$. The difference between this set of new $\delta_\ell^b(E_k)$ and the original set of total phase shifts $\delta_\ell(E_k)$ leads to a set of *estimated* $\delta_\ell^r(E_k)$, or

$$f_\ell(E_k) = \delta_\ell(E_k) - \sum_{i=0}^{i_{max}} a_i {E_k}^i. \tag{76}$$

Finally, this set of new $f_\ell(E_k)$ (or, δ_ℓ^r) are used to calculate a pair of new E_r and Γ, i.e., we interpolate the resonant energy E_r by using the simple relation

$$f_\ell(E_r) = \pi/2, \tag{77}$$

and we derive the width Γ by taking the average of two estimated values Γ_- and Γ_+, which are interpolated by using the relations

$$\begin{cases} f_\ell(E_r - \frac{\Gamma_-}{2}) &= \pi/4 \\ f_\ell(E_r + \frac{\Gamma_+}{2}) &= 3\pi/4 \end{cases} \tag{78}$$

at energies on both side of the resonance. This entire procedure is repeated iteratively until the estimated E_r and Γ are both converged. A close agreement between Γ_- and Γ_+ also assures the accuracy of the calculated E_r and Γ.

The resonant energy E_r and width Γ can also be determined from the energy variation of the probability density

$$\rho_{ns\ell}(E) = \sum_\nu \mid C_E^A(ns, \nu\ell) \mid^2 \tag{79}$$

corresponding to the singly excited $ns\ell$ ionization channel [28]. At the resonant energy E_r, the contribution to Φ_E^A from all closed channels should be at its maximum, i.e., E_r can be identified directly as the energy at which the probability density of the ionization channel $ns\ell$ is at its *minimum* value. The probability density $\rho_{ns\ell}$ is also related to the energy dependent amplitude A at large r by

$$\rho_{ns\ell}(E) \ = < \xi_{\epsilon\ell}(r) \mid \xi_{\epsilon\ell}(r) > \approx \ \frac{R}{2} A^2. \tag{80}$$

The total energy E, or the outgoing electron energy ϵ, varies as we change the radius R slightly in the CIC calculation. Since R is approximately a constant and is also substantially greater than the R-variation ΔR required to cover the resonance,

$\rho_{n\ell}(E)$ is approximately proportional to A^2. This relation, together with Eq. (61), which shows that the photoionization cross section σ is inversely proportional to A^2, suggest that σ is inversely proportional to $\rho_{n\ell}(E)$ near the resonance. As $\rho_{n\ell}(E)$ approaches its minimum value at E_r, $\sigma \rightarrow \sigma_{max}$ and as E moves away from E_r, σ decreases. Eventually, σ is reduced to half of σ_{max} when $\rho_{n\ell}(E)$ is doubled at $E_r \pm \frac{\Gamma}{2}$, where Γ is the full width at half maximum (i.e., FWHM). As a result, the positions and the widths of an entire series of doubly excited resonances can be estimated from the energy variation of the probability density of the ionization channel.

3.3.3. *Extended B-spline-based CI procedure*

To improve the accuracy of the theoretical E_r and Γ, an even larger number of configuration series representing more $\ell\ell'$ combinations are required in the CIC calculation. In particular, if the widths are to be determined from the energy variation of the phase shifts, the B spline set typically requires a size of n $\geq$ 120 at $R \sim 120a_0$ for a four- to five-digit convergence in phase shifts. Computationally, this represents a prohibitively extensive numerical effort, even with the help of the diagonalization procedure outlined in section 3.3.1. To reduce the size of the basis set, we have developed a two-step extended B-spline-based CI procedure [28].

First, a *zeroth order* CIC calcualtion is performed by including only a limited number of dominating configuration series in a basis set, which is constructed from B spline sets of n greater than 120. In addition, we carry out a similar zeroth order CI calculation with the *same* configuration series combination, which employs B spline sets of significantly smaller n ranging from 30 to 50. In our second step, a substantially larger number of configurations series of various allowed $\ell\ell'$ combinations is included in calculating E_r and Γ from the energy variation of the probability density. We are able to limit the total number of configurations of the extended basis set at a manageable level (e.g., approximately 3,000) by using the B spline sets with the *same* smaller n employed in the zeroth order calculation. The *change* in E_r and Γ due to the additional configuration series is estimated by comparing the zeroth order E_r and Γ with the ones from the extended calculation, both using the same B spline set of *smaller* n. By adding the change in E_r and Γ to the zeroth order results using B spline sets of *larger* n, we finally obtain our best estimated values for E_r and Γ. The maximum estimated uncertainty, in terms of the momentum k of the ionizaed electron, is approximately $\frac{\pi}{kR}$, which amounts to 2-5% for two-electron atoms [28].

4. Applications

Photoionization spectrum dominated by doubly excited resonances for a two-electron or a divalent atom represents perhaps one of the most direct and unambiguous atomic processes for a detailed quantitative study of the many-electron

interaction in atomic transitions. One of the best known doubly excited photoionization structures is the He $sp22^+$ ^1P resonance, which was first observed in detail by Madden and Codling [29] in He ground state photoabsorption spectrum and later classified by Cooper, Fano, and Prats [30]. Theoretically, the photionization structure of an *isolated* resonance located at resonant energy E_r is best described by the Fano formula [31] in terms of a set of resonant parameters, which includes the resonant width Γ, the asymmetry parameter q, and the nonresonant background cross section σ_b. The peak cross section σ_{max}, located at $E_{max} = E_r + \frac{1}{2}(\Gamma/q)$ according to Fano formula, equals $\sigma_b(1+q^2)$. Also, the cross section is expected to reach a zero at an energy $E_{min} = E_r - \frac{1}{2}(\Gamma q)$. Physically, the resonant profile, which is characterized by the asymmetry parameter q, measures qualitatively the interference between transitions from an initial state to the *bound* and *continuum* components of the final state wave function. If the contribution from the transition to the bound component is very small in comparison with the transition to the continuum background, q is very small and a zero cross section is expected either at or near E_r. For an intermediate q value, the resonant profile is generally asymmetric due to a comparable contribution from transitions to bound and continuum components of the final state wave function. On the other hand, if the transition is dominated by the contribution from the transition to the bound component of the state wave function, the q value is large and a more symmetric photoionization structure is expected. As a result, the q parameter, or equivalently, the resonant profile corresponding to a specific doubly excited resonance, can and often vary significantly for transitions originated from different initial states.

In constrast, the resonant width Γ, which measures the interaction strength between the bound and continuum components of the state wave function of a doubly excited autoionization state, is *independent* of the transition process. Experimentally, the width of a doubly excited autoionization state can be determined by the resonant structures originated from *any* initial states. Most of the existing measurements are limited to the photoabsorption spectra from the ground state, which are almost always strongly asymmetric due to the simultaneous change of electronic orbitals of two outer electrons in a double excitation process. For a series of broad resonances with small to intermediate q values, the standard theoretical interpretations [31,32] for an *isolated* resonance become less effective, especially when the broad resonance is also closely situated next to a second overlapping doubly excited series [33,34]. An accurate experimental determination of Γ is often difficult. For a narrow resonance, the width measurement could also be hampered by the lack of adequate energy resolution. In fact, for a two-electron atom, the resonant widths are in general more readily available from the theoretical calculations than from the experimental measuremnets.

In this section, the quantitative accuracy of the CIC method is first examined in terms of its applications to the photoionization of two-electron atoms from its ground and bound excited states. Both nonresonant and resonant absolute photoionization cross sections will be presented. Our theoretical results are compared with other available theoretical and experimental results. In the second part of this section, we present the extension of the CIC calculation to the single- and multiphoton ionization of alkaline earth atoms. Again, our theoretical results are compared

with other existing theoretical and experimental results.

4.1. *Two-electron Atoms*

The quantitative accuracy of the state wave function can be measured directly by the calculated scattering phase shift. The effect due to the electron-electron correlation to the state wave function can also be estimated by the change in phase shift as the size of the CI basis set increases. Fig. 2 presents the variaiton of the *nonresonant* e-He^+ $^{1,3}P^o$ scattering phase shifts as the basis set increases from a single $1sp$ configuration series to a total of 89 series. The phase shifts from the single ionization channel calculation, represented by the solid curves labeled as $1sp$ series only, are seen to differ significantly from our final results. The phase shift corrections due to the addition of $2sp$, $2ps$, and $2pd$ series to the $1sp$ series, account for about half of the total phase shift difference. Our calculated phase shifts, including only the 1sp, 2sp, 2ps, and 2pd series in the basis set, agree very well with the 1s2s2p close-coupling results of Norcross [36]. Between 30%-40% and approximately 25% of the phase shift difference can be attributed to the *npd*-type of configuration series for the ^{1}P and ^{3}P continua, respectively. Our converged phase shifts are in excellent agreement with the 20-state close-coupling results by Oza [37]. Our theoretical phase shifts at zero energy also approach the expected values $\pi\mu$ (where μ is the quantum defect), which equal -0.038 and 0.214 for the ^{1}P and ^{3}P series, respectively. All two-electron configuration functions included in the basis set of the nonresonant photoionization calculations are of the bound-bound or bound-continuum type, i.e., each of the two-electron basis functions in the CIC calculation consists at least one negative energy single-particle orbital function. The contribution from the continuum-continuum type of two-electron functions to the scattering phase shift in nonresonant region is negligible. Our theoretical *nonresonant* scattering phase shifts for the e-H scattering are also in excellent agreement with other earlier and more elaborate calculations (see, e.g., Fig. 2 in Ref. [6]).

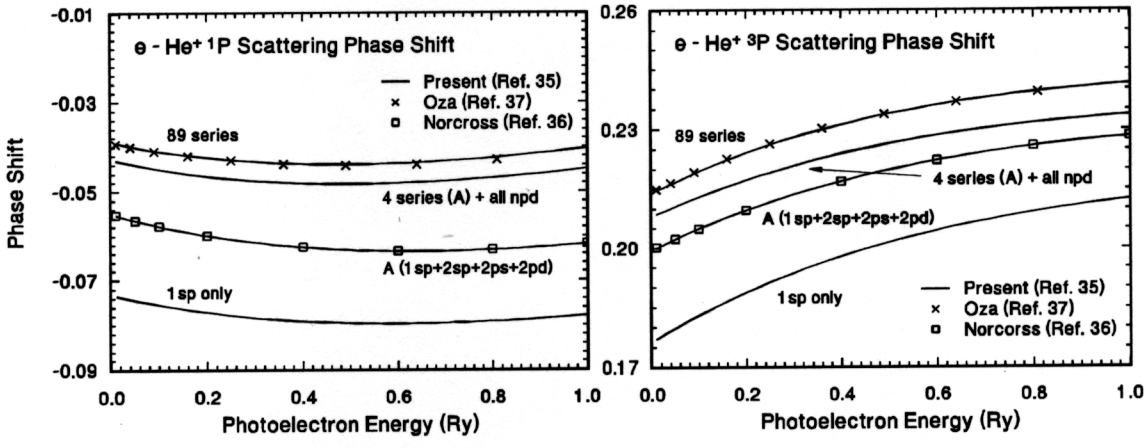

Figure 2. Variation of nonresonant e - He^+ $^{1,3}P$ scattering phase shifts as functions of photoelectron energy.

Fig. 3 presents the photoionization cross sections below the resonance structure for H^-. Our calculated photodetachment cross sections from the H^- ground state agree very well with some of the most accurate earlier theoretical calculations [2,38-40]. A simple model calculation by Crance and Aymar [41] (not shown) has led to cross sections which are significantly smaller at low energy side but too large on higher energies compared with most of the more elaborate theories. In contrast, more recent calculation, using the hyperspherical coordinates method [42], yields cross sections in the length form which are slightly higher near the peak region and slightly lower at higher energy than other theoretical results. Only the dipole-length results from the present calculation are plotted. The agreement bewteen our dipole-velocity and dipole-length results is about 1-2% or better for the entire energy range. Similarly, our calculated *nonresonant* photoionization cross sections from the ground state of He agree very well with the experimental data compiled recently by Samson [43], which are accurate to 1-2% (see, e.g., Ref. [6]).

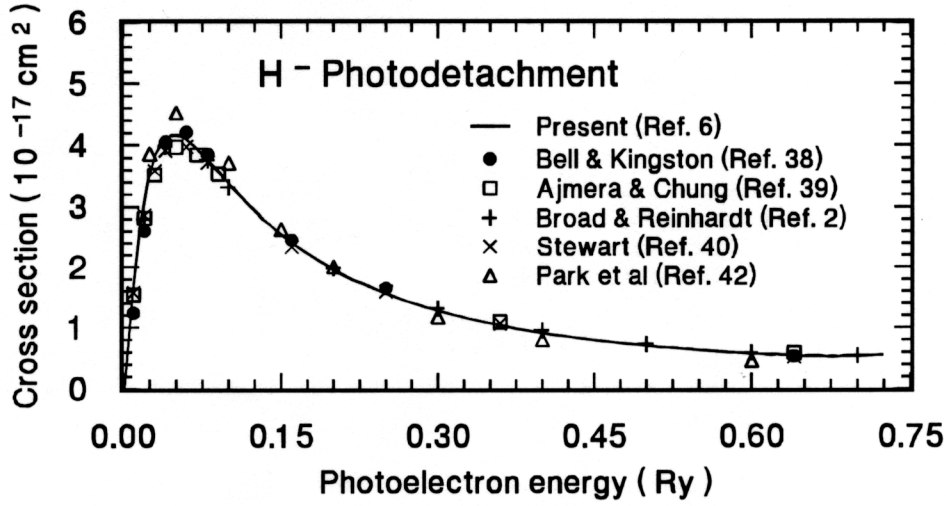

Figure 3. The photodetachment cross sections below the resonance structure for H^-.

The CIC procedure has also been applied to the nonresonant photoionization of He from 1s2s $^{1,3}S$ metastable states of He. For the 1s2s $^1S^e \rightarrow {}^1P^o$ photoionization, most of the theoretical cross sections, including the present results and those by Burgess and Seaton [44], Jacobs [45], and Dalgarno and co-workers [46], are all in close agreement with each other and they also agree well with the observed data near the ionization threshold [47,35]. Our theoretical photoionization cross sections at selected photoelectron energies are compared in detail in Table I with the close-coupling results of Jacobs [45] and Norcross [36]. At energies immediately next to the threshold, our theoretical results differ noticeably from the close-coupling calculation by Norcross [36], which employed an essentially uncorrelated initial state wave function. For the 1s2s $^3S^e \rightarrow {}^3P^o$ photoionization, our theoretical results also agree well with the existing theoretical results [44-46]. Similar to the earlier results of Burgess and Seaton [44], our near-threshold 1s2s $^3S^e \rightarrow {}^3P^o$ cross sections shown in Fig. 4 appear to be slightly less than the observed values but clearly within the experimental error bars. The ratio R between the 1s2s ^1S and 1s2s ^3S cross sections

as a function of wavelength is also shown in Fig. 4. The ratio R appears to deviate significantly from unity, especially at shorter wavelength. As a result, we could not confirm the experimental observation that the 1s2s ^{1}S cross section nearly equals the 1s2s ^{3}S cross section at energies close to the ionization threshold [47].

Table I. The nonresonant photoionization cross sections (in Mb) from He 1s2s $^{1,3}S$ metastable states. The photoelectron energy ϵ is given in Ry. Only length results are listed. (Values taken from [35].)

ϵ (Ry)	1s2s ^1S			1s2s ^3S		
	present	Jacobs [45]	Norcross [36]	present	Jacobs [45]	Norcross [36]
0.01	8.798	8.753	9.350	5.345		4.751
0.05	7.258	7.128	7.083	4.804		4.332
0.10	5.803	5.671	5.413	4.188		4.042
0.15	4.722	4.473		3.654	3.537	
0.20	3.902	3.821	3.904	3.199	3.157	3.509
0.25	3.268	3.233		2.812	2.796	
0.30	2.770	2.768		2.485	2.480	
0.40	2.047	2.068	2.122	1.968	1.970	1.993
0.60	1.225	1.233	1.258	1.302	1.311	1.268
0.80	0.795	0.794	0.858	0.913	0.926	0.918
1.00	0.546	0.543	0.490	0.671	0.685	0.629
1.20	0.390	0.388	0.319	0.512	0.527	0.500
1.40	0.285	0.284	0.277	0.404	0.418	0.449
1.60	0.212	0.211	0.219	0.328	0.342	0.372

Most of the earlier studies on the He photoabsorption spectra in the resonant region are limited to the doubly excited structures dominated by the broader $sp2n^+$ ^1P resonances. Only very recently, Domke, Remmers, and Kaindl [1] have successfully resolved in a synchrotron radiation experiment the narrow (sp,2n$^-$) and (2pnd) $^1P^o$ series, which are separated by energy differences ranging from a maximum of 16.4±0.4 meV for the 4$^-$/3d pair to an estimated 4±2 meV for the 7$^-$/6d pair. Their reported energy separations between the neighboring 2pnd and sp,2(n+1)$^-$ resonances are determined by fitting the measured photoionization spectra to a standard Fano formula [31] for the sp,2(n+1)$^-$ lines and a near symmetric monochromator function corresponding to a weighted sum of a Gaussian and a Lorentzian profile for the 2pnd lines. In addition to the early theoretical study by Burke and McVicar [23] using a four-channel close-coupling calculation over two decades ago, the (2pnd) and (sp,2n$^-$) $^1P^o$ series have been studied extensively in recent years, including a nine-channel coupled-equation calculation within the framework of many-body perturbation theory (MBPT) by Salomonson, Carter, and Kelly [48], a L^2-based R-matrix method by Gersbacher and Broad [49], and a

STO-based L^2-basis method by Sánchez and Martín [4]. These two relatively narrow $^1P^o$ series have also been studied qualitatively in other recent theoretical works, including the L^2-basis calculation by Moccia and Spizzo [3], the variational R-matrix calculation by Hamacher and Hinze [51], and the spline-based multiconfiguration Hartree-Fock (MCHF) calculation by Froese Fischer and Idrees [5].

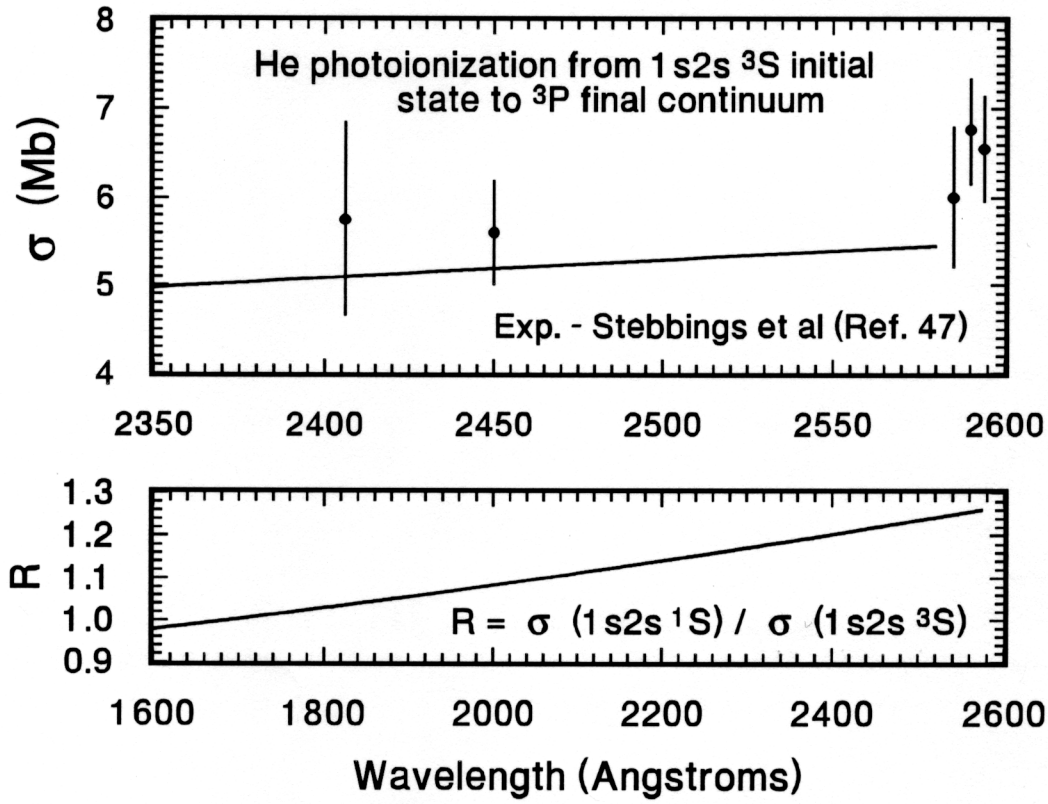

Figure 4. The near-threshold photoionization cross sections from He 1s2s ^3S metastable state and the ratio R between the 1s2s ^1S and 1s2s ^3S photoionization cross sections.

Fig. 5 presents our calculated photoionization profiles in the vicinity of the (sp,23^-), (2p3d), and (sp,24^-) $^1P^o$ resonances. The theoretical energies from our calculation have been shifted to lower energy by 3 meV for all three resonances to accommodate a direct comparison with the observed spectra. The observed spectra are normalized to the theoretical results following a procedure detailed in Ref. [7]. The calculated and the observed structure profiles appear to agree well. A hint of sharp drop to a minimum in cross section is seen on the high energy side of the sp,$2n^-$ resonances. With an energy resolution of 4 meV, it is not unexpected that the sharp dip in cross section (with a "width" less than 2 meV) next to the 2p3d resonance is not observed experimentally. Similarly, the top portion of the resonance structures are also absent in the observed profiles when their widths become less than 2 meV. Except for minor quantitative details, the calculations by Salomonson, Carter, and Kelly [48] and Sánchez and Martín [4] have also suggested asymmetric

Table II. The resonance energies E_r of selected He (sp,2n−) and (2pnd) $^1P^o$ resonances and their energy separations Δ below the N=2 threshold. The numbers in parentheses are experimental errors in units of the last digits. The energy separation given by a[-b] = a×10^{-b} eV. The energy in eV is converted using the factor employed in Ref. [1], i.e., 1 Ry = 13.60503 eV and IP_∞ = 79.0078 eV.

State	Observed [1]	Present	Oza [37]	Ho [52]	Sanchez & Martin [50]
		——	E_r (eV)	——	
3^-	62.7580(2)	62.7611	62.7611	62.7611	62.757
2p3d	64.1189(2)	64.1217		64.1211	64.118
4^-	64.1353(2)	64.1377	64.1379	64.1374	64.134
2p4d	64.6485(4)	64.6514		64.6512	64.648
5^-	64.6574(2)	64.6598	64.6599	64.6598	64.656
		——	Δ (eV)	——	
$3^-/4^-$	1.3773(4)	1.3766	1.3768	1.3763	1.377
$4^-/5^-$	0.5221(4)	0.5221	0.5220	0.5224	0.522
3d/4d	0.5296(6)	0.5297		0.5301	0.530
4^-/3d	16.4(4)[-3]	16.0[-3]		16.3[-3]	16.0[-3]
5^-/4d	8.9(6)[-3]	8.4[-3]		8.6[-3]	8.0[-3]

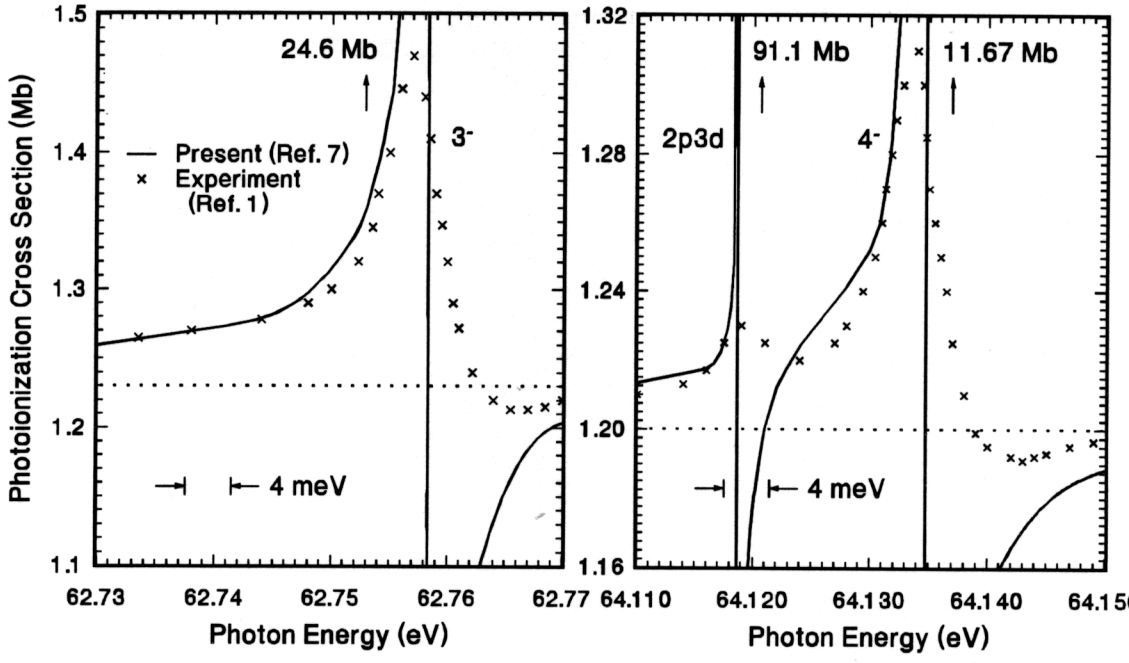

Figure 5. Comparison of the calculated and the observed photoionization cross sections near the doubly excited $(sp, 23^-)$, $(2p3d)$, and $(sp, 24^-)$ ^1P resonances of He atom below the N=2 threshold.

resonance profile for the 2pnd series with a significantly larger negative q value than the one for the sp,2n$^-$ series. Together with our result, we conclude that, in contrast to the observed spectra, a higher peak photoionization cross section σ_{max} is expected for the 2pnd resonances than that for the sp,2n$^-$ resonances. In Table II, we compare the observed resonant energies and the energy separations for the He (2pnd) and (sp,2n$^-$) ^1P series with the results from the present calculation and a few other recent theoretical results. Some of the calculated resonant energies are modified to account for the use of different energy-conversion factors. The overall agreement between experiment and theory is excellent. The numerical resonant widths and the peak photoionization cross sections σ_{max} from ground state to selected (sp,2n$^+$), (sp,2n$^-$), and (2pnd) $^1P^o$ series belown the He$^+$ N=2 threshold are given in Ref. [7].

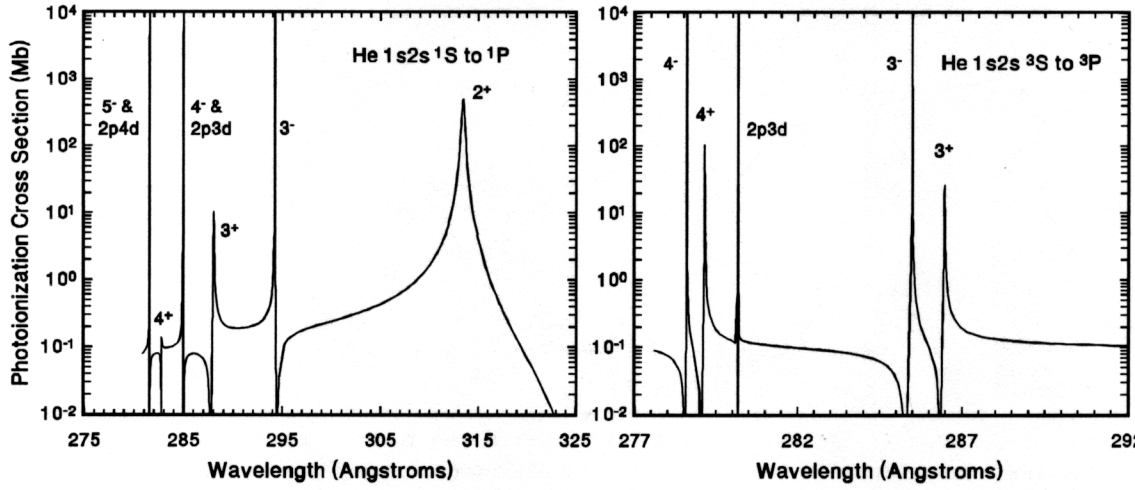

Figure 6. Photoionization spectra from He 1s2s $^{1,3}S$ metastable states to $^{1,3}P$ doubly excited resonances.

In contrast to the strongly asymmetric ground state spectrum, the resonant profiles are more symmetric in general for bound excited states spectra with peak cross sections that are several orders of magnitude greater than the cross sections from the ground state, such as the He 1s2s $^1S \rightarrow$ sp22$^+$ ^1P reported in Ref. [6]. This suggests that, experimentally, both Γ and E_r of a doubly excited resonance can be determined, perhaps less ambiguously, from photoionization of bound excited states. Recent development in high-resolution monochromator operating with high synchrotron radiation intensity [1] may have opened up the experimental possibility in resonant region, at least for those resonances with high peak cross sections, if high density bound excited He atoms can be generated. In Fig. 6 we present our calculated photoionization spectra from He 1s2s $^{1,3}S^e$ metastable states to the resonant region dominated by the $^{1,3}P^o$ doubly excited resonances. Similar to the ^{1}P photoionization spectra from the 1s^2 ^{1}S ground state [1,7], the sp,2(n+1)$^-$ and 2pnd ^{1}P resonances are separated by approximately 16 meV and 9 meV for the n=3 and 4 pairs, respectively. Except for the sp,2n$^+$ ^{1,3}P series, the *peak* cross sections σ_{max} for the narrower sp,2n$^-$ and 2pnd ^{1,3}P states are significantly larger than the nonresonant photoionization cross sections.

The peak cross sections σ_{max} for selected transitions are listed in Table II of Ref. [35]. For the 1s2s ^{1}S $\rightarrow$ sp,22$^+$ ^{1}P transition, our theoretical σ_{max} = 519.3 Mb is in agreement with the calculated value of 541 Mb by Dalgarno and co-workers [46], but differ noticeably from the close-coupling results of 436 Mb and 384 Mb by Norcross [36] and Jacobs [45], respectively. Since σ_{max} is inversely proportional to Γ (see, e.g., Eq. (46) of Ref. [53]), this disagreement may be partially attributed to the approximately 15% overestimation in width from the close-coupling calculations in comparison with most of the existing theoretical values shown in Table III of Ref. [35]. For the 1s2s ^{3}S $\rightarrow$ sp,22$^+$ ^{3}P transition, our theoretical σ_{max} = 2554 Mb is greater than the results from all three previous calculations [36,45,46]. This discrepancy can be attributed *entirely* to the difference in the calculated resonant widths (see, e.g., Table IV of Ref. [35]). In fact, the σ_{max} would range from 2400 to 2500 Mb for these three calculations if adjustment due to the difference in resonant width is taken into account.

For a doubly excited $(n\ell_i\nu\ell_o)\ ^{2S+1}L$ autoionization state embedded in a *singly ionized* $(1s\epsilon\ell)\ ^{2S+1}L$ continuum background corresponding to an ionized ℓ electron of energy ϵ, the resonant width Γ is *qualitatively* related to the Coulomb interaction between the bound and continuum components of the state wave function, i.e., it is approximately proportional to

$$|< (n\ell_i\nu\ell_o)\ ^{2S+1}L \mid \frac{1}{r_{12}} \mid (1s\epsilon\ell)\ ^{2S+1}L >|^2 \ . \tag{81}$$

Theoretically, the ν-dependence of the resonant widths Γ of a series of $(n\ell_i\nu\ell_o)\ ^{2S+1}L$ doubly excited resonances is approximately given by the ν-dependence of the one-electron radial function of the $\nu\ell_o$ orbit. In fact, if the range of the effective interaction r_0 is small in comparison with the effective principal quantum number ν, i.e., for a small r_0/ν, it can be shown that Γ is given qualitatively by [54]

$$\sum_{i=1} \frac{c_i}{\nu^{2i+1}} \ , \tag{82}$$

where c_i are constants independent of ν. As ν increases along the autoionization series, Γ should approach a ν^{-3}-dependence. This ν^{-3}-dependence is illustrated in Fig. 7 for the dominating odd-parity He $(sp, 2n^+)\ ^{1,3}P$ series. Specifically, our calculated resonant widths, expressed in terms of the product of Γ and ν^3 as functions of effective principal quantum number ν, are compared with the results of a few of the earlier and more recent theoretical calculations. For the ^1P series, our calculation agrees very well with the complex-coordinate rotational calculation by Ho [52]. The agreement with the 20-state close-coupling calculation by Oza [37] is also very good, except for the small but noticeable drop for the $(sp, 24^+)\ ^1P$ state in the close-coupling result. The results of the earlier truncated-diagonalization method [12] and the 3-state close-coupling calculation [23] appear to diviate from the results of the more elaborate recent calculations. For the ^3P series, the overall agreement between our calculation and the complex-coordinate rotational calculation by Ho [55] and the 20-state close-coupling calculation by Oza [37] is excellent. Detailed tabulations of the resonant energies and widths are given elsewhere [35].

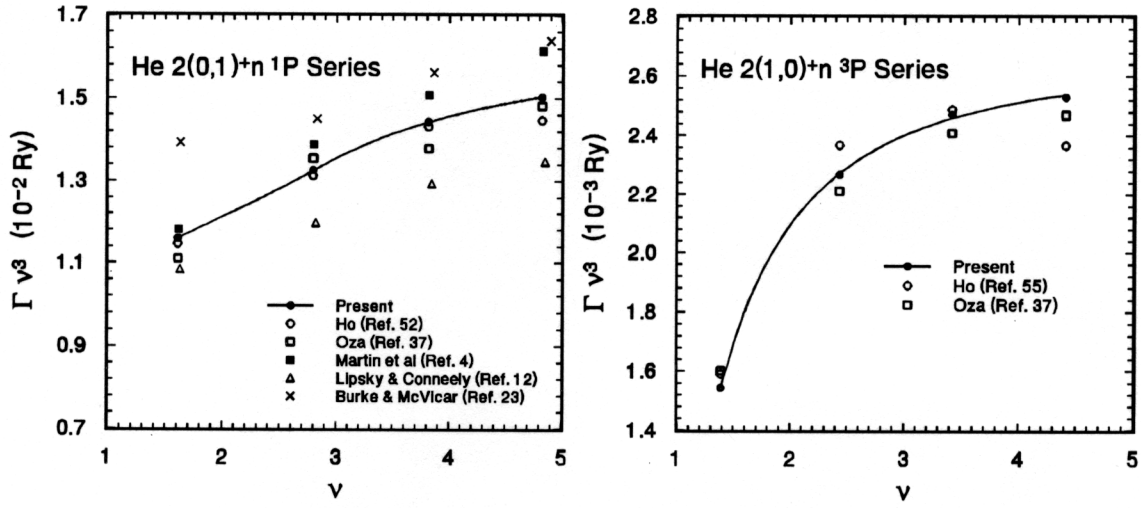

Figure 7. The variation of the product of resonant width Γ and ν^3 as function of the effective principal quantum number ν for the He $2(0,1)^+n\ ^1P$ and $2(1,0)^+n\ ^3P$ autoionization series. The solid curve represents a least square fit of the present results to Eq. (82).

4.2. *Divalent Atoms*

In Fig. 8, our calculated photoionization cross sections of neutral Mg from its ground state [8] are compared with the earlier theoretical results by Moccia and Spizzo [3] and the most recent *absolute* photoabsorption cross sections measured by Yih *et al* [56]. Our results are also consistent with the normalized experimental data by Preses *et al* [57]. In addition, our results are in close agreement with other earlier theoretical results, including the velocity results by Bates and Altick [24] and the MCHF results by Froese Fischer and Saha [5], although all the above mentioned theoretical results are noticeably less than the results from the earlier version of the R-matrix method by O'Mahony and Greene [58] at energy near the ionization threshold. The CIC procedure has also been applied to photoionization from the bound excited states of Mg [8]. In Fig. 9, we present our calculated cross sections for the direct photoionization from the $3s3p^1P$ bound excited state of Mg at energies close to the $3p^2\ ^1S$ autoionization state. Our theoretical result is in excellent agreement with the observed data compiled from an earlier two-color two-step experiment [59]. To present a direct comparison, the experimental results are normalized against the theoretical cross sections at the peak value. Our calculated length and velocity results agree to better than 5%. Only the length results are shown in Fig. 9.

In Fig. 10, we present the results of our photoionization calculations for the Be-like C^{++} [60]. Our calculation has shown that in contrast to the prominent asymmetric structure in the vicinity of the 2pnd ^1P resonance, the cross section exhibits a near zero dip close to the 2pns ^1P autoionization state, which corresponds to a $q \approx 0$ type of Fano profile. On the other hand, for transitions from a 2sns ^1S

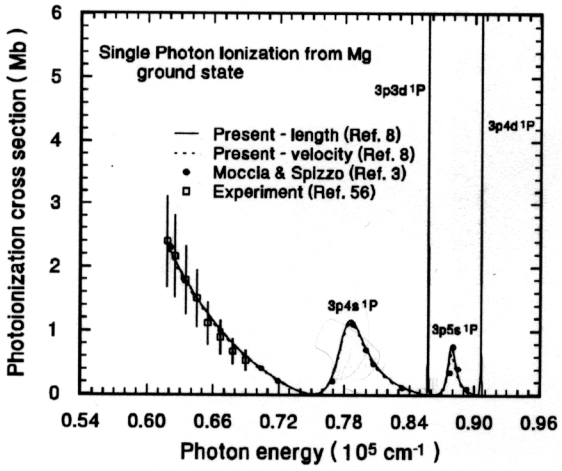

Fig. 8 Photoionization cross section leading to ^1P continuum from the ground state of Mg.

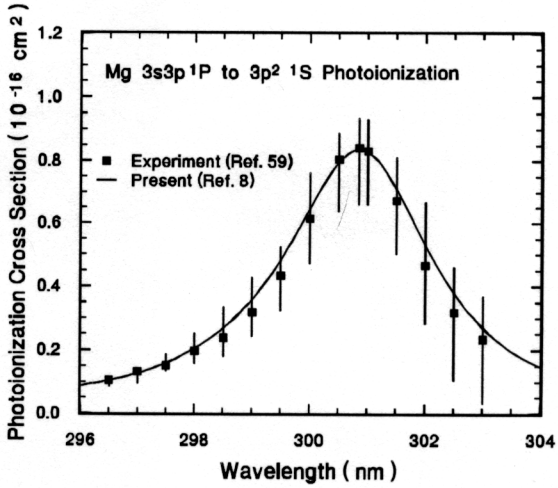

Fig. 9 Photoionization cross section from the singly excited $3s3p\ ^1P$ state of Mg to the doubly excited $3p^2\ ^1S$ resonance in the continuum.

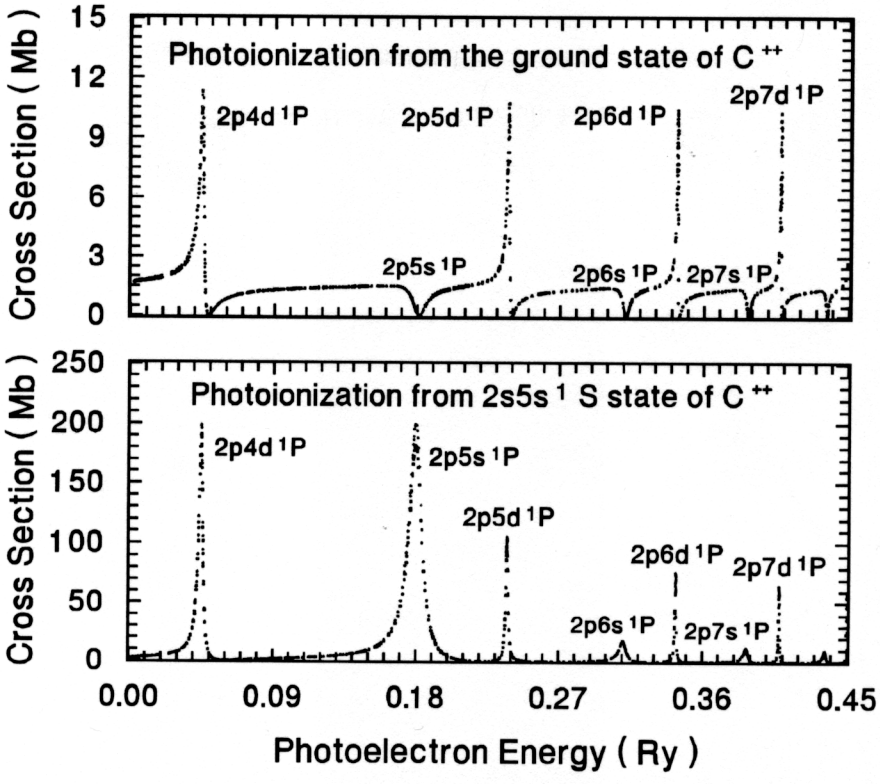

Figure 10. Photoionization cross sections from the $2s^2\ ^1S$ ground state and the $2s5s\ ^1S$ bound excited state of Be-like C^{++} ion. (Data taken from [60].)

bound excited state, the cross section close to the 2pns ^{1}P resonance is represented by a nearly symmetric profile, which corresponds to a large q value resonance structure due to a direct 2s $\rightarrow$ 2p transition. Similar to the earlier examples, once again, the spectra shown in Fig. 10 has led us to conclude that, experimentally, both the resonant width and energy of a doubly excited autoionization state may be determined less ambiguously from photoionization of bound excited states.

Fig. 11 presents our theoretical generalized cross sections in 10^{-50} cm^4-sec from the ground state of Mg for linearly polarized one-color two-photon processes [8], i.e.,

$$\begin{aligned} Mg(3s^2\,{}^1S) + 2\hbar\omega &\longrightarrow Mg^{**}(3pn\ell\,{}^1S \text{ or } {}^1D) \\ &\longrightarrow Mg^{+}(3s\,{}^2S) + e^{-}. \end{aligned} \tag{83}$$

The results of our Mg two-photon ionization calculation are in close agreement with an earlier L^2-basis calculation by Moccia and Spizzo [3]. Our calculation has shown that the two-photon ionization spectrum leading to the ^1S continuum is dominated by the strong resonant structure due to the 3s3p ^{1}P intermediate state and the 3pnp ^{1}S autoionization series. As for the ^{1}D continuum, only a hint of the 3pnp ^{1}D autoionization series is seen, in contrast to the narrow but visible 3pnf ^{1}D series. The 3s3p ^{1}P intermediate resonant structure remains strong. A few of the final state autoionization structures shown in Fig. 11, including 3p4p ^{1}S, 3p5p ^{1}S and 3p4f ^{1}D states, have been observed recently by Shao and Charalambidis at Crete [61]. The fact that the 3pnp ^{1}D series is not observed experimentally is consistent with the absence of prominent structure for the 3pnp ^{1}D series in our calculated spectrum. A total of 12 configuration series are included in our calculation.

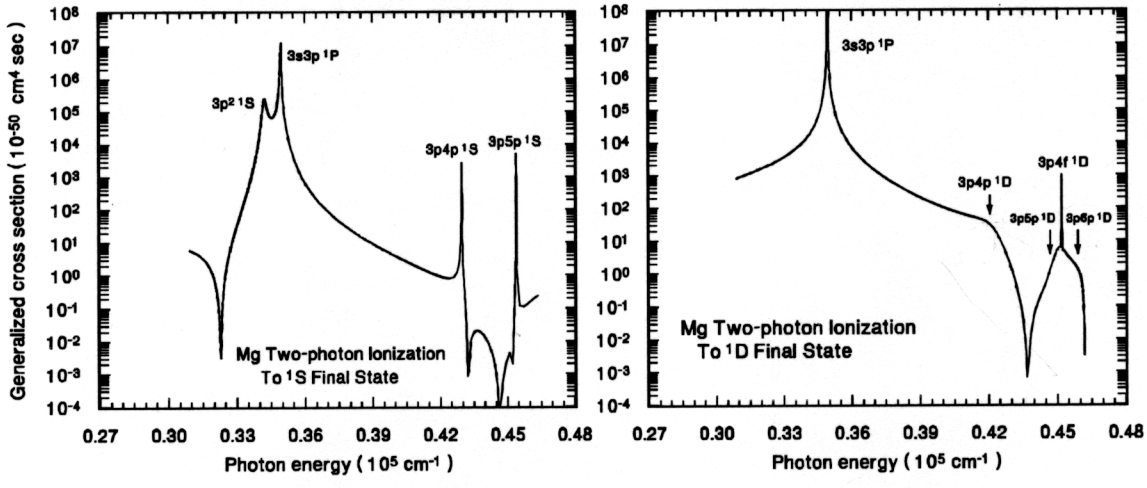

Figure 11. The calculated generalized cross sections for two-photon ionization leading to ^1S and ^1D continua from the ground state of Mg. (Data taken from [8].)

In Fig. 12, we present the generalized cross sections for linearly polarized one-color three-photon ionization of Mg from ground state that lead directly to the ^{1}P

and ^{1}F continua. For the three-photon ionization leading to the ^{1}P continuum, the prominent doubly excited 3pns ^{1}P resonant states, which dominate the one-photon process, are completely overwhelmed by the 3sns ^{1}S and 3snd ^{1}D intermediate resonant structures. In fact, the broad 3p4s ^{1}P structure seen in the single photoionization spectrum (see, e.g., Fig. 8) is reduced to a slightly broaden shoulder at the low energy side of the 3s5s ^{1}S intermediate resonance in the three-photon spectrum. For the three-photon ionization leading to the ^{1}F continuum, the spectrum is dominated by the resonant structures due to the 3snd ^{1}D intermediate bound excited states. The strongly correlated 3p3d ^{1}F doubly excited autoionization states [62] is less prominent but remains visible on the low energy side of the 3s6d ^{1}D intermediate resonance. Again, a total of 12 configuration series is included in our state wave functions calculation for all bound and continuum states. The length and velocity results are nearly indistinguishable on the logarithmic plot.

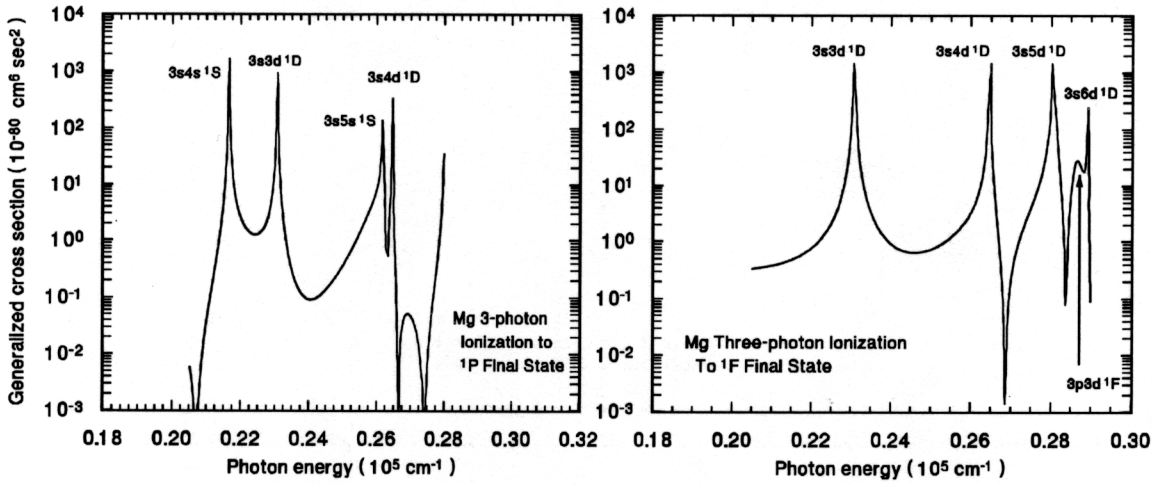

Figure 12. The calculated generalized cross sections for three-photon ionization leading to ^1P and ^1F continua from the ground state of Mg. (Data taken from [8].)

Our theoretical calculation has clearly shown that as the number of photon increases, the energy spectrum of a *single-color* multiphoton process does not necessarily reveal the atomic structure effects which dominate the final state multi-electron interactions in the continuum, in spite of its ability to reach directly the higher-L states of both odd and even parity. In fact, a *multi-color* multi-step process may turn out to be a more efficient physical mechanism in the study of multi-electron interactions in the continuum if it is capable of yielding detail photoionization data for transition from a highly correlated bound excited state to a strongly correlated autoionization state.

The applications of the CIC method to two-electron and divalent atoms presented in this section have successfully demonstrated the effectiveness of this approach in leading to accurate theoretical spectra in a single continuum. Extensions to spectra in multi-continua and more complicated atoms are currently in progress.

Acknowledgments

This work was supported by NSF under Grant No. PHY91-11420.

References

[1] M. Domke, G. Remmers, and G. Kaindl, Phys. Rev. Letters **69**, 1171 (1992).

[2] E. J. Heller, W. P. Reinhardt, and H. A. Yamani, J. Comp. Phys. **13**, 536 (1973); J. T. Broad and W. P. Reinhardt, Phys. Rev. A**14**, 2159 (1976); E. J. Heller and H. A. Yamani, Phys. Rev. A**9**, 1201 (1974); Phys. Rev. A**9**, 1209 (1974); J. J. Wendoloski and W. P. Reinhardt, Phys. Rev. A**17**, 195 (1978).

[3] R. Moccia and P. Spizzo, J. Phys. B**18**; 3537 (1985)

[4] F. Martin and A. Salin, Chem. Phys. Lett. **157**, 146 (1989); I. Sánchez and F. Martin, J. Phys. B**23**, 4263 (1990).

[5] C. Froese Fischer and H. P. Saha, Can. J. Phys. **65**, 772 (1987); C. Froese Fischer and M. Idrees, J. Phys. B**23**, 679 (1990);

[6] T. N. Chang and X. Tang, Phys. Rev. A**44**, 232 (1991).

[7] T. N. Chang, Phys. Rev. A**47**, 3441 (1993).

[8] T. N. Chang and X. Tang, Phys. Rev. A**46**, R2209 (1992).

[9] H. A. Bethe and E. E. Salpeter, **Quantum Mechanics of One- and Two-electron Atoms**, (Springer-Verlag, Berlin, 1957).

[10] T. N. Chang and E. T. Bryan, Phys. Rev. A**38**, 645 (1988).

[11] T. N. Chang and Y. S. Kim, Phys. Rev. A**36**, 2609 (1986).

[12] L. Lipsky and A. Russek, Phys. Rev. **142**, 59 (1966); L. Lipsky and M. J. Conneely, Phys. Rev. A**14**, 2193 (1976).

[13] R. Z. Zare, J. Chem. Phys. **45**, 1966 (1966); **47**, 3561 (1967).

[14] T. N. Chang and K. T. Chung, Chinese J. Phys. **27**, 425 (1989).

[15] T. N. Chang, Phys. Rev. A**39**, 4946 (1989).

[16] C. Laughlin and G. A. Victor, in *Atomic Physics 3*, edited by S. J. Smith and G. K. Walters, (Plenum, New York, 1973), p. 247.

[17] C. H. Greene and L. Kim, Phys. Rev. A**36**, 2706 (1987).

[18] W. R. Johnson, S. A. Blundell, and J. Sapirstein, Phys. Rev. A**37**, 307 (1988).

[19] C. deBoor, *A Practical Guide to Splines*, (Springer, NY, 1978).

[20] T. N. Chang, in *Relativistic, Quantum Electrodynamics, and Weak Interaction Effects in Atoms*, edited by W. Johnson, P. Mohr, and J. Sucher, AIP Conf. Proc. No. 189, (American Institute of Physics, New York, 1989), p. 217.

[21] T. N. Chang, Phys. Rev. A**36**, 447 (1987).

[22] A. Burgess, Proc. Phys. Soc. **81**, 442 (1963).

[23] P. G. Burke and D. D. McVicar, Proc. R. Soc. London **86**, 989 (1965).

[24] G. Bates and P. L. Altick, J. Phys. B**6**, 653 (1973).

[25] A. L'Huillier, X. Tang, and P. Lambropoulos, Phys. Rev. A**39**, 1112 (1989).

[26] X. Tang, T. N. Chang, P. Lambropoulos, S. Fournier, and L. F. Dimauro, Phys. Rev. A**41**, 5265 (1990).

[27] E. R. Davidson, J. Comp. Phys. **17**, 87 (1975).

[28] T. N. Chang, Phys. Rev. A**47**, 705 (1993).

[29] R. P. Madden and K. Codling, Astrophys. J. **141**, 364 (1965).

[30] J. W. Cooper, U. Fano, and F. Prats, Phys. Rev. Lett. **10**, 518 (1963).

[31] U. Fano, Phys. Rev. **124**, 1866 (1961).

[32] D. W. Norcross and M. J. Seaton, J Phys. B**9**, 2983 (1976).

[33] J. M. Esteva, G. Mehlman-Balloffet, and J. Romand, J. Quant. Spectrosc. Radiat. Transfer, **12**, 1291 (1972).

[34] G. Mehlman-Balloffet and J. M. Esteva, Astrophys. J. **157**, 945 (1969).

[35] T. N. Chang and M. Zhen, Phys. Rev. A**47**, 4849 (1993).

[36] D. W. Norcross, J Phys. B**4**, 652 (1971).

[37] D. H. Oza, Phys. Rev. A**33**, 824 (1986).

[38] K. L. Bell and A. E. Kingston, Proc. Phys. Soc. London **90**, 895 (1967).

[39] M. P. Ajmera and K. T. Chung, Phys. Rev. A**12**, 475 (1976).

[40] A. L. Stewart, J. Phys. B**11**, 3851 (1978).

[41] M. Crance and M. Aymar, J. Phys. B**18**, 3529 (1985).

[42] C. H. Park, A. F. Starace, J. Tan, and C. D. Lin, Phys. Rev. A**33**, 1000 (1986).

[43] J. A. R. Samson, Phys. Rep. **28**, 303 (1976); and private communication (1990).

[44] A. Burgess and M. J. Seaton, Mon. Not. R. Astron. Soc. **120**, 121 (1960).

[45] V. L. Jacobs, Phys. Rev. A**3**, 289 (1971); **4**, 939 (1971); **9**, 1938 (1974).

[46] A. Dalgarno, H. Doyle, and M. Oppenheimer, Phys. Rev. Letters **29**, 1051 (1972); H. Doyle, M. Oppenheimer and A. Dalgarno, Phys. Rev. A**11**, 909 (1975).

[47] R. F. Stebbings, F. B. Dunning, F. K. Tittel, and R. D. Rundel, Phys. Rev. Letters **30**, 815 (1973).

[48] S. Salomonson, S. L. Carter, and H. P. Kelly, Phys. Rev. A**39**, 5111 (1989).

[49] R. Gersbacher and T. Broad, J Phys. B**23**, 365 (1990).

[50] I. Sánchez and F. Martín, J. Phys. B**23**, 4263 (1990).

[51] P. Hamacher and J. Hinze, J. Phys. B**22**, 3397 (1989).

[52] Y. K. Ho, Z. Phys. D, Atoms, Mol, and Clusters **21**, 191 (1991).

[53] T. N. Chang, Phys. Rev. A**37**, 4090 (1988).

[54] T. N. Chang, J Phys. B**11**, L583 (1978).

[55] Y. K. Ho, Phys. Rev. A**23**, 2137 (1981); and preprint (1993).

[56] T. S. Yih, H. H. Wu, H. T. Chan, C. C. chu, and B. J. Pong, Chinese J. Phys. **27**, 136 (1989).

[57] J. M. Preses, C. E. Burkhardt, W. P. Garver, and J. J. Leventhal, Phys. Rev. A**29**, 985 (1984).

[58] P. F. O'Mahony and C. H. Greene, Phys. Rev. A**31**, 250 (1985).

[59] R. E. Bonanno, C. W. Clark, and T. B. Lucatorto, Phys. Rev. A**34**, 2082 (1986).

[60] T. N. Chang and L. Zhu, preprint (1993).

[61] Y. L. Shao and D. Charalambidis, private communication.

[62] T. N. Chang and X. Tang, Phys. Rev. A**38**, 1258 (1988).